



**José Miguel
Cardoso da Silva**

**Medição e modelação de difusividades de compostos
bioativos em líquidos comprimidos**

**Measurement and modeling diffusivities of bioactive
compounds in compressed liquids**



**José Miguel
Cardoso da Silva**

**Medição e modelação de difusividades de compostos
bioativos em líquidos comprimidos**

**Measurement and modeling diffusivities of bioactive
compounds in compressed liquids**

Dissertação apresentada à Universidade de Aveiro para cumprimento dos requisitos necessários à obtenção do grau de Mestre em Engenharia Química, realizada sob a orientação científica do Doutor Carlos Manuel Santos da Silva, Professor Associado do Departamento de Química da Universidade de Aveiro e coorientação da Doutora Maria Inês Purcell de Portugal Branco, Professora Auxiliar do Departamento de Química da Universidade de Aveiro.

o júri

presidente

Doutor Francisco Avelino Silva Freitas
Professor Auxiliar do Departamento de Química da Universidade de Aveiro

Doutora Ana Luísa Carvalho Magalhães
Técnica de Laboratório da Sakthi Portugal SP21

Doutor Carlos Manuel Santos da Silva
Professor Associado do Departamento de Química da Universidade de Aveiro

agradecimentos

Gostaria de agradecer a todos os membros do grupo EgiChem pelo acolhimento, amizade e apoio demonstrado ao longo destes últimos meses. Um obrigado especial aos meus orientadores, Doutor Carlos Manuel Silva e à Doutora Inês Portugal, não só por todo o empenho, motivação e conhecimento que me transmitiram nestes últimos meses, mas também por todo o apoio e amizade ao longo destes cinco anos. Um obrigado também ao Bruno Zêzere por toda a ajuda e apoio na realização desta dissertação.

Agradeço também aos meus pais por toda a motivação e confiança que me deram ao longo destes cinco anos. Sem o seu apoio, com certeza que não teria conseguido chegar até aqui. A eles um muito obrigado.

Por fim, um obrigado a todas as pessoas que se cruzaram comigo durante este percurso e que sempre me deram força e motivação para continuar a crescer pessoal e profissionalmente.

palavras-chave

Acetato de etilo, Astaxantina, Difusão, Etanol, Licopeno, Modelação

resumo

Na última década, a crescente preocupação global com a saúde, tratamento e prevenção de doenças levou a uma rápida expansão do mercado dos compostos bioativos, o que induziu as indústrias farmacêutica, cosmética e alimentar a investir na extração e recuperação dessas moléculas.

O mercado global dos compostos bioativos ultrapassou os 27 mil milhões de dólares em 2015 e estima-se que em 2024 atinja os 51.71 mil milhões.

Muitas separações industriais, tais como extrações sólido-líquido e extrações supercríticas, são frequentemente limitadas por fenómenos de transferência de massa e, portanto, há uma grande necessidade de conhecer os coeficientes de difusão para poder modelar, projetar e otimizar esses processos adequadamente. Nesse sentido, a presente dissertação tem como objetivo a medição e modelação do coeficiente de difusão de dois compostos bioativos de interesse, nomeadamente, licopeno em etanol e astaxantina em acetato de etilo.

Para realizar a medição das difusividades a diluição infinita utilizou-se o método cromatográfico de abertura de pico (CPB), num intervalo de temperaturas de 303.15 a 333.15 K e num intervalo de pressão de 1 a 100 bar. Os valores de difusividade obtidos encontram-se entre 3.447×10^{-6} e 6.679×10^{-6} $\text{cm}^2 \text{s}^{-1}$ para o licopeno e entre 8.172×10^{-6} e 1.223×10^{-5} $\text{cm}^2 \text{s}^{-1}$ para a astaxantina.

Posteriormente, os valores de difusividade obtidos foram analisados em função da sua dependência com a temperatura, pressão, densidade do solvente e as coordenadas de Stokes-Einstein. Por fim, os resultados foram modelados usando vários modelos da literatura. Os coeficientes de difusão calculados e experimentais foram comparados com base no desvio relativo absoluto médio (AARD). Os valores apresentam desvios que variam entre 5.00 e 91.29 % para o licopeno e 3.94 e 79.38 % para a astaxantina.

Para ambos os compostos constatou-se que as equações empíricas e semi empíricas de Magalhães *et al.*, com desvios de 5.00 a 8.92 % e 3.94 a 7.29 % (para o licopeno e astaxantina, respetivamente), o modelo de volume livre de Dymond-Hildebrand-Batchinsky (DHB), com desvios de 9.78 e 4.80 % (para o licopeno e astaxantina, respetivamente) e o modelo híbrido Tracer Liu-Silva-Macedo com 1 parâmetro (TLSM_d), com desvios de 6.92 e 6.37 % (para o licopeno e astaxantina, respetivamente) são as mais adequadas para descrever a difusividade dos compostos estudados.

keywords

Astaxanthin, Diffusion, Ethanol, Ethyl acetate, Lycopene, Modeling

abstract

Over the last decade, the growing concern about global health, treatment and disease prevention has led to a rapid expansion of the market of bioactive compounds, which induced the pharmaceutical, cosmetics and food industries to invest in the extraction and recovery of such molecules.

The global market for bioactive compounds has exceeded 27 billion dollars by 2015 and it is estimated to reach 51.71 billion dollars by 2024.

Many industrial separations, such as solid-liquid and supercritical extractions, are often limited by mass transfer phenomena, and thus there is a great need to know diffusion coefficients in order to model, design and optimize these processes properly. In this sense, the main objective of this dissertation was the measurement and modeling of diffusion coefficients of two bioactive compounds of interest, namely, lycopene in ethanol and astaxanthin in ethyl acetate.

To perform the diffusivity measurements at infinite dilution, it was used the chromatographic peak broadening (CPB) method, in the temperature range of 303.15 to 333.15 K and pressure range of 1 to 100 bar. The diffusivity values obtained are between 3.447×10^{-6} and 6.679×10^{-6} $\text{cm}^2 \text{s}^{-1}$ for lycopene and between 8.172×10^{-6} and 1.223×10^{-5} $\text{cm}^2 \text{s}^{-1}$ for astaxanthin.

Subsequently, the measured diffusivities were analyzed as a function of their dependence on temperature, pressure, solvent density, and in Stokes-Einstein coordinates. Finally, the results were modeled using several models from the literature. The calculated and experimental diffusion coefficients were compared based on the average absolute relative deviation (AARD). The values exhibit deviations varying between 5.00 and 91.29 % for lycopene and 3.94 and 79.38 % for astaxanthin.

For both compounds it was verified that the empirical and semi-empirical equations of Magalhães *et al.*, with deviations of 5.00 to 8.92 % and 3.94 to 7.29 % (for lycopene and astaxanthin, respectively), the free volume model of Dymond-Hildebrand-Batchinsky (DHB) with deviations of 9.78 and 4.80 % (for lycopene and astaxanthin, respectively) and the hybrid 1-parameter Tracer Liu-Silva-Macedo correlation (TLSM_d), with deviations of 6.92 and 6.37 % (for lycopene and astaxanthin, respectively) are most suitable to describe the diffusivity of the studied compounds.

Content

Content	I
Figure index.....	III
Table index	V
Nomenclature.....	VII
Chapter 1 - Motivation and thesis structure	1
Chapter 2 - Methods for binary diffusion coefficients (D_{12}) measurement	5
2.1 Chromatographic Peak Broadening (CPB) method.....	5
2.2 Chromatographic Impulse Response (CIR) technique	12
2.3 Modified Taylor-Aris technique.....	15
Chapter 3 - Modeling tracer diffusion coefficients	17
3.1 Models based on the free volume theory.....	17
Dymond-Hildebrand-Batschinski (DHB) correlation	18
3.2 Models based on the hydrodynamic theory.....	18
Stokes-Einstein relation.....	19
Wilke-Chang equation.....	19
Scheibel equation.....	20
Tyn-Calus equation	20
Lai-Tan equation.....	21
Reddy-Doraiswamy model.....	22
3.3 Models based on the rough hard sphere theory	22
Catchpole-King correlation	23
3.4 Hybrid models.....	24
Predictive model TLSM	24
TLSM _d correlation (one parameter)	25
3.5 Empirical and semi-empirical correlations of Magalhães <i>et al.</i>	26
Chapter 4 - Experimental section	27
4.1 Equipment and procedure.....	27
4.2 Solutes and measurement conditions.....	29

4.3 Properties of the solvents	30
Density of liquid ethanol	30
Viscosity of liquid ethanol	31
Density of liquid ethyl acetate.....	31
Viscosity of liquid ethyl acetate	32
Chapter 5 - Results and discussion.....	33
5.1 Experimental equipment validation	33
5.2 Tracer diffusivity of lycopene in ethanol	34
5.3 Tracer diffusivity of astaxanthin in ethyl acetate	39
5.4 Modeling the experimental values of D_{12}	43
Chapter 6 - Conclusion and future work suggestions	47
References	49
Appendix A - Chemical compounds	58
Appendix B - Properties estimation	59
Appendix C - Absorbance spectra.....	60

Figure index

Figure 1.1- Diagram adaptation of a typical supercritical fluid extraction (SFE) system and of typical pressurized liquid extraction (PLE) system.....	2
Figure 2.1- Adaptation of the schematic diagram of the CPB method.....	6
Figure 2.2- Schematic representation of the velocity profile inside a coiled tube.	9
Figure 2.3- Schematic diagram of the CIR technique.	13
Figure 2.4- Schematic diagram of the modified Taylor-Aris technique.....	16
Figure 4.1- Schematic representation of the equipment used to perform the measurements of the D_{12}	28
Figure 5.1- Comparison between the measured values (●) and the literature values (■) of D_{12} of the gallic acid.....	34
Figure 5.2- Determination of the optimal wavelength (λ) at 1 bar and 323.15 K, to study the diffusivity of lycopene in ethanol.....	35
Figure 5.3- Experimental response curve (×) and calculated curve (–) for lycopene in ethanol ($\lambda = 255$ nm) at 1 bar and 323.15 K.....	36
Figure 5.4- D_{12} of lycopene in ethanol as function of pressure for several temperatures..	37
Figure 5.5- D_{12} of lycopene in ethanol as function of the solvent density for several temperatures.....	38
Figure 5.6- D_{12} of lycopene in ethanol plotted in Stokes-Einstein coordinates for several temperatures.....	39
Figure 5.7- Determination of the optimal wavelength (λ) at 1 bar and 313.15 K, to study the diffusivity of astaxanthin in ethyl acetate.....	40
Figure 5.8- Experimental response curve (×) and calculated curve (–) for astaxanthin in ethyl acetate ($\lambda = 460$ nm) at 1 bar and 333.15 K	41
Figure 5.9- D_{12} of astaxanthin in ethyl acetate as function of pressure for several temperatures.....	42

Figure 5.10- D_{12} of astaxanthin in ethyl acetate as function of the solvent density for several temperatures.	42
Figure 5.11- D_{12} of astaxanthin in ethyl acetate plotted in Stokes-Einstein coordinates for several temperatures.	43
Figure 5.12- Calculated versus experimental values of D_{12} of lycopene in (a) and (b) and of astaxanthin in (c) and (d).	45
Figure C. 1- Lycopene absorbance spectrum ranging from 190 to 440 nm.	60
Figure C. 2- Astaxanthin absorbance spectrum ranging from 190 to 690 nm.	60

Table index

Table 4.1- Characteristics of the diffusion column used in the experimental work.	28
Table 5.1- Experimental and literature values of D_{12} of the gallic acid and their relative error.	33
Table 5.2- Experimental conditions, experimental D_{12} of lycopene in ethanol obtained through the CPB method and calculated density and viscosity of the solvent.	37
Table 5.3- Experimental conditions, experimental D_{12} of astaxanthin in ethyl acetate obtained through the CPB method and calculated density and viscosity of the solvent.	41
Table 5.4- Modeling results of D_{12} of lycopene in ethanol and astaxanthin in ethyl acetate.	44
Table A. 1- List of the chemical compounds used in the experimental work.	58
Table A. 2- Strutural formulas of the compounds used in the experimental work.	58
Table B. 1- Properties of the chemical compounds used in this work.	59

Nomenclature

Symbol	Description	Units
$Ab_{S_{\max}}$	Maximum absorbance	(Dimensionless)
A_{peak}	Peak area	(Dimensionless)
b_{V_D}	Optimized parameter from the DHB model correction	(mol m ⁻³)
B_{DHB}	Interaction solute-solvent parameter in the DHB model	(cm ⁻¹ mol ⁻¹ s ⁻¹ K ^{-0.5})
C	Mass concentration	(kg m ⁻³)
c	Concentration of the solute	(mol m ⁻³)
\bar{c}	Calculated average radial concentration of the solute	(mol m ⁻³)
c_0	Total injected concentration	(mol m ⁻³)
c_i	Molar concentration of component i	(mol m ⁻³)
c^{exp}	Concentration of solute at the column exit	(mol m ⁻³)
C_n	Number of carbons	(Dimensionless)
D	Dispersion coefficient	(m ² s ⁻¹)
D_{11}	Self diffusion coefficient of the solvent	(m ² s ⁻¹)
D_{12}	Tracer diffusion coefficient of solute 2 through solvent 1	(m ² s ⁻¹)
$D_{c,11}$	Self diffusion coefficient of the solvent at the critical point	(m ² s ⁻¹)
De	Dean's number, ($De = Re\zeta^{-0.5}$)	(Dimensionless)
F	Force	(kg m s ⁻²)
H	Theoretical plate height	(m)
$J_{2,z}$	Molar flux of a solute 2 in the z direction	(m ² mol s ⁻¹)
k	Retention factor	(Dimensionless)
$k_{12,d}$	Binary interaction constant	(Dimensionless)
k_B	Boltzmann constant	(1.38064852×10 ⁻²³ J K ⁻¹)
L	Length of the column	(m)
m	Total amount of solute injected	(mol)

m_{V_D}	Optimized parameter from the DHB model correction	($\text{m}^3 \text{mol}^{-1} \text{K}^{-1}$)
M_i	Molecular weight of component i	(g mol^{-1})
M_{12}	Reduced molecular weight of the system	(Dimensionless)
N_A	Avogadro's number	($6.0221409 \times 10^{23} \text{mol}^{-1}$)
n_D	Refractive index	(Dimensionless)
p	Pressure	($\text{kg m}^{-1} \text{s}^{-2}$)
p_0	Atmospheric pressure	($\text{kg m}^{-1} \text{s}^{-2}$)
Pe_x	Longitudinal Peclet's number, ($Pe_x = \bar{u}LD_{12}^{-1}$)	(Dimensionless)
p_c	Critical pressure	($\text{kg m}^{-1} \text{s}^{-2}$)
P_i	Parachor of component i	($\text{cm}^{3.25} \text{g}^{0.25} \text{s}^{-0.5}$)
r	Radial coordinate	(m)
R	Ideal gas constant	($8.3144621 \text{J mol}^{-1} \text{K}^{-1}$)
R_0	Internal radius of the column	(m)
R_c	Radius of the coil of the column	(m)
Re	Reynolds's number, ($Re = \rho\bar{u}2R_0\mu^{-1}$)	(Dimensionless)
R_p	Radius of the particle	(m)
S	Zeroth moment	($\text{mol dm}^{-3} \text{s}$)
Sc	Schmidt's number, ($Sc = \mu(\rho D_{12})^{-1}$)	(Dimensionless)
t	Time	(s)
\bar{t}	Average retention time	(s)
t_0	Retention time of the inert species	(s)
t_i	Time at 10 % of the peaks high used in the fitting method	(s)
t_r	Retention time	(s)
t_{tr}	Retention time of the tracer	(s)
T	Temperature	(K)
T_b	Temperature at the normal boiling point	(K)
T_{br}	Reduced temperature at the normal boiling point	(K)
T_c	Critical temperature	(K)
T_r	Reduced temperature of the system	(Dimensionless)
$T_{r,i}^*$	Reduced temperature for component i using LJ energy	(Dimensionless)
u	Velocity of the particle	(m s^{-1})

\bar{u}	Average solvent's velocity	(m s ⁻¹)
u_{opt}	Optimal velocity	(m s ⁻¹)
ν	Mobility of the particle	(s kg ⁻¹)
V_c	Critical molar volume	(m ³ mol ⁻¹)
V_d	Atomic diffusion volume	(m ³)
V_i	Molar volume of component i	(m ³ mol ⁻¹)
V_{in}	Intrinsic molar volume	(m ³ mol ⁻¹)
V_D	Minimum molar volume	(m ³ mol ⁻¹)
$W_{0.607}$	Half width of the peak in time units	(s)
x_i	Molar fraction of the component i	(Dimensionless)
z	Axial coordinate	(m)
z'	Axial coordinate corrected by the movement of the fluid	(m)

Greek letters

Symbol	Description	Units
γ_i	Surface tension of component i	(kg m s ⁻²)
$\delta(z)$	Dirac's function	(Dimensionless)
ε	Square root of the mean square error	(Dimensionless)
$\varepsilon_{i,LJ}$	Lennard-Jones energy parameter of component i	(K)
ζ	Curvature ratio, ($\zeta = R_c R_0^{-1}$)	(Dimensionless)
λ	Wavelength	(nm)
μ_0	Reference viscosity	(kg m ⁻¹ s ⁻¹)
μ_i	Viscosity of component i	(kg m ⁻¹ s ⁻¹)
κ	Thermal conductivity	(W (m K) ⁻¹)
ρ_0	Reference density	(kg m ⁻³)
ρ_i	Density of component i	(kg m ⁻³)
ρ_c	Critical density	(kg m ⁻³)
$\rho_{n,1}$	Solvent number density	(m ⁻³)
$\rho_{r,i}$	Reduced density of component i	(Dimensionless)
$\rho_{rn,1}^*$	Reduced number density of the solvent	(Dimensionless)
σ^2	Variance	(m ²)

$\sigma_{i,LJ}$	Lennard-Jones diameter of component i	(m)
$\sigma_{i,eff}$	Effective hard sphere diameter of component i	(m)
ϕ	Association factor of the solvent	(Dimensionless)

Subscripts

Symbol	Description
0	Initial condition
1	Solvent
2	Solute
12	Binary
eff	Effective
i	Component i
LJ	Lennard-Jones

Superscripts

Symbol	Description
I	Input
II	Output
calc	Calculated
exp	Experimental

Abbreviations

Symbol	Description
AARD	Average absolute relative deviation
BPR	Back pressure regulator
CPB	Chromatographic peak broadening
CIR	Chromatographic impulse response
DHB	Dymond-Hildebrand-Batchinsky
EU	European Union
LJ	Lennard-Jones
LSM	Liu-Silva-Macedo

NDP	Number of data points
NMR	Nuclear magnetic resonance
PEEK	Poly(ether ether ketone)
PCS	Photon correlation spectroscopy
PLE	Pressurized liquid extraction
RTR	Radioactive tracer response
SC-CO ₂	Supercritical carbon dioxide
SD	Solid dissolution
SFC	Supercritical fluids
SFE	Supercritical fluids extraction
TLSM	Tracer Liu-Silva-Macedo predictive model
TLSM _d	Tracer Liu-Silva-Macedo 1 parameter correlation
USA	United States of America
UV	Ultraviolet

Chapter 1

Motivation and thesis structure

Over the last decade, the growing concern about global health, the increase in consumers' demand for naturalness and the trend towards plant based-food have led to a higher demand for bioactive compounds and a renewed interest in fruits and vegetables from the industry and the scientific community [1-3].

Bioactive compounds are molecules that show certain biological effects and act as functional ingredients when present in low concentrations in an organism. These metabolites are different from the primary ones because they are not essential for the growth, development and reproduction of the organism. However, they still play an important role, since their presence improves the overall health of the organism [4]. Based on their chemical structures, bioactive compounds can be classified into several different groups, such as phenolic acids and polyphenols, alkaloids, carotenoids, terpenes and terpenoids, flavonoids, tannins, anthocyanins, amino acids and proteins, fatty acids and lipids, polysaccharides and essential oils [5-7].

Over the years, the benefits of the consumption of bioactive compounds in a regular basis have been shown, due to their antiaging [8], anticancer [6], antidiabetic [9], antihypertensive [10], antimicrobial [11], antioxidant [8,9,11,12], cardioprotective [6,8,11,12], neuroprotective properties and immunoregulatory activity [11].

Due the above-mentioned properties, the market of the bioactive compounds has suffered a rapid expansion, leading the pharmaceutical, cosmetic and food industries to invest in the extraction and recovery of these compounds from a wide range of sources, such as fruits, vegetables, herbs, algae, eggs and many others [5,9,13].

In 2015, the global market of the bioactive compounds had exceeded 27.0 billion dollars and it is expect to reach 51.71 billion dollars by 2024 [14].

Notwithstanding the environmental and economic sustainability, industries are always looking to reduce manufacturing costs by the valorization of by-products. Since the agroindustry and fishing industry produce a high amount of waste, the resulted by-products of these industries can be used as a reliable, cheap, sustainable, profitable and eco-compatible source to obtain bioactive compounds. However, the extraction process is the key point for a successful recovery of bioactive compounds [5].

Extraction of natural products has been used since ancient times. Many different civilizations, such as Egyptians, Greeks, Romans and Aztecs, possessed extraction processes to produce perfumes, medicines or food. Nowadays, it is almost impossible to find a production process in the food, cosmetic, perfume, pharmaceutical or fine chemicals industries, which does not use extraction processes [15].

The competitiveness and the globalization of the markets and the environment protection require constant technological innovations, allowing modern extraction techniques, such as supercritical fluids extraction (SFE) and pressurized liquid extraction (PLE), to replace traditional extraction methods. These modern extraction techniques can be more selective, ecofriendly, fast and present better extraction yields than the traditional ones [5].

It is shown below on Figure 1.1 the typical system's schematics of the SFE and the PLE.

Many industrial separations, such as supercritical fluid and solid-liquid extractions, are often limited by film and/or intraparticle mass transfer. This means that there is a big necessity of knowing the transport properties in order to model, design and optimize these processes properly, specially the diffusion coefficient (D_{12}).

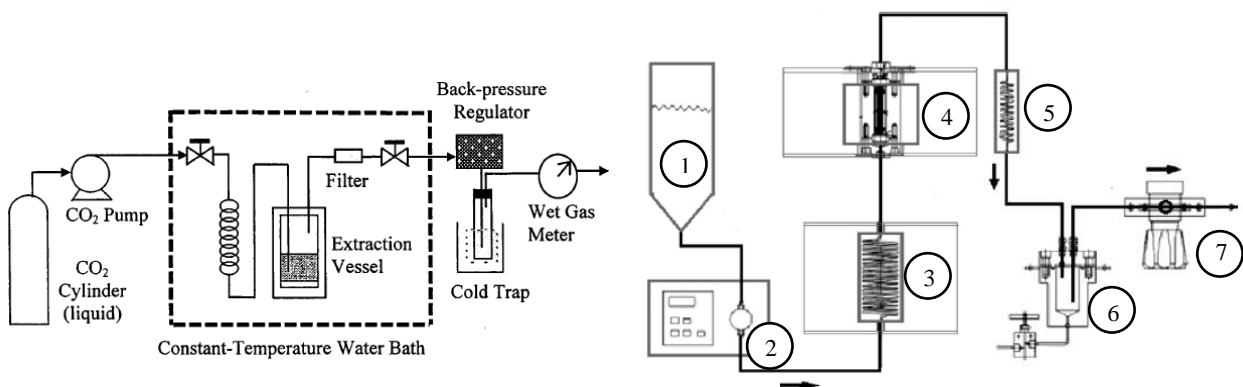


Figure 1.1– Diagram adaptation of a typical supercritical fluid extraction (SFE) system (left panel) [16] and of typical pressurized liquid extraction (PLE) system (right panel) [17]. (1) Solvent's tank, (2) high pressure pump, (3) pre-heater, (4) main heater with a reactor, (5) chiller, (6) solid/liquid separator and (7) back pressure regulator.

Mass transfer can be defined as the molecular movement of a species in a mixture from one location to another. This phenomenon can occur through two main mechanisms, by diffusion or convection. While diffusion consist in random and spontaneous microscopic movements of molecules, convection can be described as the macroscopic fluid motion [18].

Mass diffusion can occur in liquids, gases and solids, but since it is heavily influenced by the average intermolecular distance (and temperature), diffusion is faster in gases, than in liquids and than in solids [19]. This phenomenon is mathematically described by Fick's first law, which was derived by Fick in 1855, as an analogy to Fourier's first law of heat conduction [20]. This law uses concentration gradient as driving force, which is an approximation. In fact, the accurate driving force to mass transfer is the chemical potential gradient [21].

Fick's law applied to binary mixtures is described by:

$$J_{2,z} = -D_{12} \frac{dc_2}{dz} \quad (\text{Eq. 1.1})$$

where $J_{2,z}$ is the molar flux of a solute 2 in the z direction, c_2 is molar concentration of the solute 2 and D_{12} is the diffusion coefficient of a solute 2 through the solvent 1.

Fick's law resumes the three basic principles of mass diffusion. These principles are [18]:

- i. Mass transfer occurs because there are concentration gradients; this mean that in a binary mixture, the species diffuse from higher to lower concentration regions.
- ii. The mass transfer rate is proportional to the area normal to the mass transfer direction. Thus, the rate can be express as a flux.
- iii. Once there are no concentration gradients, which means the concentration uniformity was reached, the mass transfer stops (in the case of binary mixtures).

Despite the great advances in modern extraction techniques over the past decade, there is still a lack of accurate D_{12} data. In this sense, the present dissertation aims to respond to this absence of data through the measurement and subsequent modeling of the diffusion coefficient of lycopene in ethanol and the diffusion coefficient of astaxanthin in ethyl acetate. In this study, the D_{12} values were measured in the range 1-100 bar and 303.15-333.15 K.

Lycopene ($C_{40}H_{56}$) is an open chain, unsaturated, red-colored carotenoid that occurs naturally in fruits and vegetables such as tomatoes, watermelons, papayas, asparagus and

pink grapefruits [12,22]. This compound is solid at atmospheric conditions and is currently approved as a food coloring in the European Union (EU) [23] and in the United States of America (USA) [24]. Lycopene is particularly interesting to the chemical, food and pharmaceutical industries due its bioactive properties. Several studies have shown that lycopene consumption can prevent heart diseases and many types of cancer [12,22,25-29]. According to the last report of the European Commission, Portugal is the third highest producer of tomato in the EU [30]. The recovery of lycopene from tomato wastes can be a good opportunity to valorize by-products and minimize the waste produced by this industry.

Astaxanthin ($C_{40}H_{52}O_4$) is also an interesting bioactive compound with relevant antioxidant properties. Over the years, the benefits of this compound have been associated with reduced risk of diseases, such as age-related macular degeneration and ischemic diseases. This xanthophyll carotenoid is a violet solid at atmospheric conditions that can be found in many microorganisms and marine animals, such as shrimp, crayfish, salmon, trout, krill, microalgae or even in yeast [10,29,31-33]. According to the European Commission, Portugal is the country that consumes the most fishery products in the EU. On average, a Portuguese citizen eats 56.8 kg of fish per year, while the average EU citizen only eats 24.9 kg per year [34]. The residues of the fishing industry can be a profitable, reliable and sustainable source to obtain astaxanthin.

Thesis structure

The present dissertation is divided into six chapters. In Chapter 2 it is described the different experimental methods to measure the D_{12} , as well as an analysis of the theoretical background of the method used in the current work. In Chapter 3 are presented the models used to represent/estimate the obtained data. In Chapter 4 it is described the experimental procedure followed during this work as well as the equipment and chemicals used. In Chapter 5, the obtained results are presented and discussed. These values are also compared with calculations from literature models. At last, in Chapter 6 are presented the main conclusions of this thesis and suggestions for a future work.

Chapter 2

Methods for binary diffusion coefficients (D_{12}) measurement

The binary diffusion coefficient (D_{12}) of organic compounds in pressurized systems cannot be determined with the traditional methods of measuring transport properties, since these methods do not adapt well at high pressures. Thus, there are five different methods to obtain diffusivity data in pressurized systems [35]: solid dissolution (SD) technique; chromatographic peak broadening (CPB) method; photon correlation spectroscopy (PCS); nuclear magnetic resonance (NMR) spectroscopy; radioactive tracer response (RTR).

In the current work, the technique used to measure the D_{12} was the CPB method. Its theoretical background is discussed below. It is also focused the basis of the modified Taylor dispersion method and the chromatographic impulse response (CIR) method, which are improvements to the original CPB technique [36].

2.1 Chromatographic peak broadening (CPB) method

The chromatographic peak broadening (CPB) method is also called Taylor dispersion method and is the most used experimental technique to measure diffusion coefficients [35,37,38].

This method is based on the fundamental work of Taylor [39-41] that was further developed later by Aris [42]. Taylor's study was focused on the dispersion of a solute in a laminar steady-state flow of a mobile phase through a tube of uniform diameter.

Although this method was not specifically thought to be used as a basis for the measurement of diffusion coefficients [43], this technique was firstly used by Giddings and Seager [44] to measure D_{12} values of gases at low pressures. Later it was extended to dense

gases by Balenovic *et al.* [45], to liquids by Ouano [46] and to supercritical fluids (SCF) by Swaid and Schneider [47].

In the CPB method, a sharp and small pulse is injected into a carrier fluid or mixture that is flowing under laminar steady-state through a tube of uniform diameter [35,43,48] as it is shown in Figure 2.1.

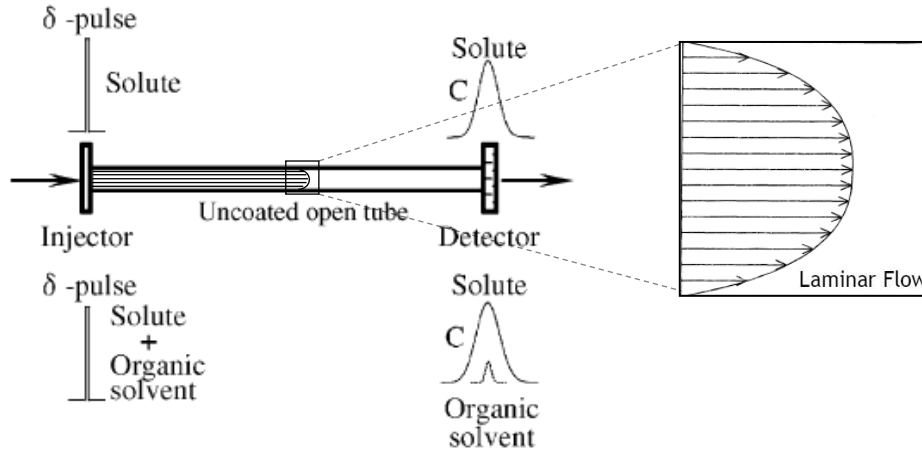


Figure 2.1- Adaptation of the schematic diagram of the CPB method [36].

Taylor showed that the injected peak would broaden along the tube due to the combined action of the solvent's axial convection and the molecular diffusion in the radial direction. The axial dispersion is negligible due to the long tubes implied [41].

If mutual diffusion was insignificant, the pulse would exhibit a parabolic profile, meaning that molecules near the tube wall would be almost stagnant while particles in the center would be moving much faster (twice the average linear velocity), resulting in a widely dispersed peak registered at the detector [43]. At the other extreme, if D_{12} had a very large value, the detector would record the original injected peak because the solute would experience all different streamlines very quickly, making them to move at the average solvent velocity. Thus, when a widely dispersed peak is recorded, it is expected that the diffusion coefficient of the solute is very small while large values are expected for narrower pulses [48].

The dispersion of the injected pulse can be mathematically described by Eq. 2.1 [41],

$$\frac{\partial c}{\partial t} = D_{12} \left[\frac{1}{r} \cdot \frac{\partial}{\partial r} \cdot \left(r \frac{\partial c}{\partial r} \right) + \frac{\partial^2 c}{\partial z^2} \right] - 2\bar{u} \cdot \left(1 - \frac{r^2}{R_0^2} \right) \cdot \frac{\partial c}{\partial z} \quad (\text{Eq. 2.1})$$

where D_{12} is the binary diffusion coefficient, c is the concentration of the solute (also called tracer), R_0 is the internal radius of the tube, \bar{u} is the average solvent velocity, t is the time, and r and z are the radial and axial distances, respectively.

As mentioned before, the axial dispersion is neglected, since the time necessary to observe relevant concentration variations due to this mechanism is very long when compared to radial diffusion. The longitudinal or axial Peclet number, $Pe_x = \bar{u} L D_{12}^{-1}$, relates characteristic convective and diffusion times [49]. Thus, the axial diffusion term in Eq. 2.1 is neglected when this dimensionless number assumes very high values. To be more precise, Taylor defined Eq. 2.2 as the limiting condition to neglect the axial dispersion term [41], where L is the length of the tube.

$$\frac{L}{\bar{u}} \gg \frac{R_0^2}{3 \cdot 8^2 D_{12}} \quad (\text{Eq. 2.2})$$

Applying this approximation to Eq. 2.1, it is obtained:

$$\frac{\partial c}{\partial t} = D_{12} \left[\frac{1}{r} \cdot \frac{\partial}{\partial r} \cdot \left(r \frac{\partial c}{\partial r} \right) \right] - 2\bar{u} \cdot \left(1 - \frac{r^2}{R_0^2} \right) \cdot \frac{\partial c}{\partial z} \quad (\text{Eq. 2.3})$$

The initial and boundary conditions are shown below, where m is the injected amount of tracer and $\delta(z)$ is the Dirac's function.

$$\text{at } t = 0, \quad c = \frac{m}{\pi R_0^2} \delta(z) \quad (\text{Eq. 2.4})$$

$$\text{at } r = 0 \text{ and } r = R_0, \quad \frac{\partial c}{\partial r} = 0 \quad (\text{Eq. 2.5})$$

$$\text{at } z = \pm\infty, \quad c = 0 \quad (\text{Eq. 2.6})$$

The average concentration over cross sectional area of tubing is calculated by:

$$\bar{c}(z, t) = \frac{2}{R_0^2} \int_0^{R_0} c(r, z, t) r dr \quad (\text{Eq. 2.7})$$

Taylor and Aris showed the asymptotic behavior of Eq. 2.3 is described by [49]:

$$\frac{\partial \bar{c}}{\partial t} + \bar{u} \frac{\partial \bar{c}}{\partial z} = D \frac{\partial^2 \bar{c}}{\partial z^2} \quad (\text{Eq. 2.8})$$

where D is a dispersion coefficient. In his solution, Taylor neglected axial diffusion but Aris showed that it can be incorporated into Taylor's model by adding the molecular diffusion coefficient to the coefficient calculated by Taylor, as shown below in Eq. 2.9 [36,50,51]. This simplification restricts the mathematical validity of the model to tubes of infinite length.

$$D = D_{12} + \frac{R_0^2 \bar{u}^2}{48 D_{12}} \quad (\text{Eq. 2.9})$$

Taking a closer look at Eq. 2.9 it is possible to see that any increase in the solvent velocity or the tube radius leads to an increase in the dispersion. On the other hand, the dispersion value reduces with the increase of D_{12} , as long as $R_0^2 \bar{u}^2 (48 D_{12})^{-1} \gg D_{12}$.

Defining a new axial variable, z' , as axial distance variable on the moving coordinate at the average solvent velocity, $z' = z - \bar{u}t$, and applying it to Eq. 2.8 it is obtained:

$$\frac{\partial \bar{c}}{\partial t} = D \frac{\partial^2 \bar{c}}{\partial z'^2} \quad (\text{Eq. 2.10})$$

where the initial and boundary condition are:

$$\text{at } t = 0, \bar{c} = \frac{m}{\pi R_0^2} \delta(z') \quad (\text{Eq. 2.11})$$

$$\text{at } z' = \pm\infty, \bar{c} = 0 \quad (\text{Eq. 2.12})$$

The analytical solution is given by [49,51]:

$$\frac{\bar{c}}{c_0} = \frac{1}{2\sqrt{\pi Dt}} \exp\left[-\frac{(z - \bar{u}t)^2}{4Dt}\right] \quad (\text{Eq. 2.13})$$

The concentration profile at the end of the column, resulting from the solute's injection, can be mathematically described in terms of a peak variance in units of length by:

$$\sigma^2(z) = \frac{2DL}{\bar{u}} = \frac{2D_{12}L}{\bar{u}} + \frac{R_0^2 \bar{u}L}{24D_{12}} = LH \quad (\text{Eq. 2.14})$$

where σ^2 is the variance and H is the theoretical plate height [35]. This theoretical plate height can be calculated by Eq. 2.15, where $W_{0.607}$ is the half width of the peak in time units, measured at 60.7 % of the peak height [35,49] and t_r is the retention time.

$$H = \frac{LW_{0.607}^2}{t_r^2} = \frac{\bar{u}W_{0.607}^2}{L} \quad (\text{Eq. 2.15})$$

According to Levenspiel and Smith [52], the concentration profile at the end of the tube is essentially gaussian if the following condition is fulfilled [43]:

$$\frac{D}{\bar{u}L} < 0.01 \quad (\text{Eq. 2.16})$$

Both Eqs. 2.14 and 2.16 were derived for straight tubes. However, since the length of the tube required, for the application of the chromatographic methods to be accurate, is quite long [47,48], the tube has to be coiled. This way, the tube can be placed at constant temperature inside an oven or a bath. Due to the coiling, the velocity profile inside the tube is elongated. Additionally, once the velocity at the center of the tube hits the maximum value, the fluid is thrown out, and since mass accumulation cannot occur, it is generated a flow in centrifugal way causing a double helix where the fluid moves, as shown in Figure 2.2 [49].

These centrifugal effects increase the mixing inside the tube, resulting in higher diffusional effects, that are traduced in narrower peaks and larger apparent values of D_{12} [48].

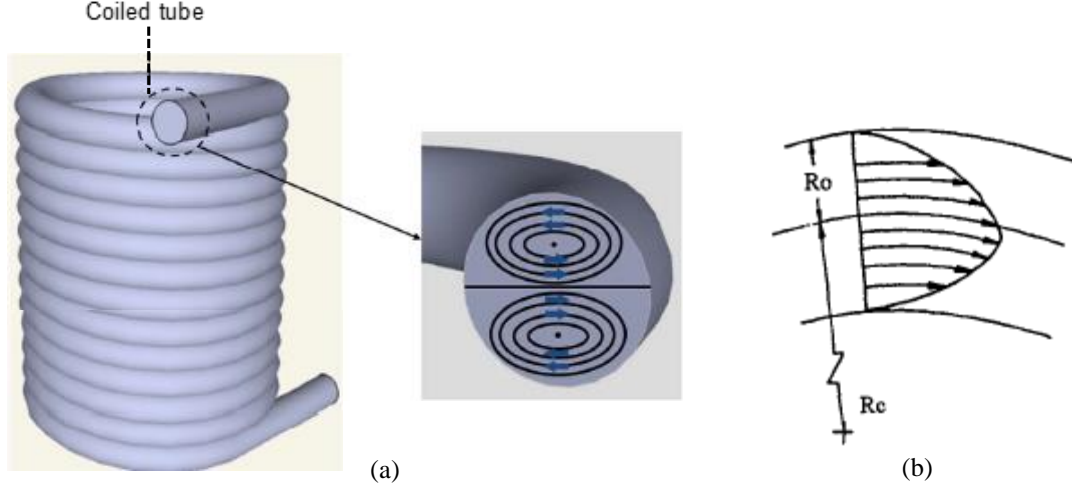


Figure 2.2- Schematic representation of the velocity profile inside a coiled tube. In (a) is a schematic representation of the secondary circulatory motion in the tube cross section (adapted from [53]). In (b) is a schematic representation of the velocity profile of a laminar flow inside the tube (adapted from [49]). (R_0 is the internal radius of the tube and R_c is the radius of the coil).

Due to the tube's coiling, there are deviations to Taylor-Aris model. These deviations can be expressed as functions of Reynolds (Re) and Schmidt (Sc) numbers and by a geometric factor, the curvature ratio (ζ). These values can be calculated by Eqs. 2.17, 2.18 and 2.19 respectively. Under certain conditions, Re and ζ are not independent variables; in fact, Dean's number (De), which is defined by Eq. 2.20, expresses the relation between centrifugal forces and inertial forces and determines the dispersion behavior [43,49].

$$Re = \frac{\rho \bar{u} 2R_0}{\mu_1} \quad (\text{Eq. 2.17})$$

$$Sc = \frac{\mu_1}{\rho D_{12}} \quad (\text{Eq. 2.18})$$

$$\zeta = \frac{R_c}{R_0} \quad (\text{Eq. 2.19})$$

$$De = \frac{Re}{\sqrt{\zeta}} \quad (\text{Eq. 2.20})$$

Nunge *et al.* [54] showed that the peak broadening effect is proportional to $Re^2 Sc \zeta^{-2}$ and this effect dominates at lower Reynolds numbers if $\zeta < 10$. In contrast, the peak narrowing effect is proportional to $(De^2 Sc)^2$ and dominates at higher Reynolds numbers [48,55].

Focusing on the secondary flow effects, Moulijn *et al.* [50] and Alizadeh *et al.* [55] showed that these effects can be neglected if the following restriction is fulfilled [43,56]:

$$De\sqrt{Sc} < 10 \quad (\text{Eq. 2.21})$$

In order to ensure an error below 1 %, Funazukuri *et al.* suggested that the previous restriction should be lower than 8 instead of 10 [56].

Since small temperature or pressure changes can occur on connection between the dispersion column and detector, van der Laan showed that these perturbations can be neglected if Eq. 2.22 is fulfilled [57].

$$\frac{\bar{u}L}{D} > 1000 \quad (\text{Eq. 2.22})$$

If the conditions imposed by Eqs. 2.16, 2.21 and 2.22 are satisfied, the Taylor-Aris model is valid for coiled tubes, and rearranging Eq. 2.14 is possible to calculate D_{12} through Eq. 2.23. On this equation, H is calculated by Eq. 2.15 [35].

$$D_{12} = \frac{\bar{u}}{4} \left[H \pm \sqrt{H^2 - \frac{R_0^2}{3}} \right] \quad (\text{Eq. 2.23})$$

According to Giddings and Seager [44], the negative root of Eq. 2.23 only has physical meaning when the fluid velocity inside the tube is higher than the optimal velocity, u_{opt} ; this velocity is the one that minimizes H and is calculated by Eq. 2.24.

Taking into consideration that the optimal velocity is usually very small for liquids and supercritical fluids, and that it can be easily exceeded when working with dense fluids, the negative root should be used in these cases. For velocities below u_{opt} , it should be chosen the positive root of the equation [43].

$$u_{opt} = \sqrt{48} \frac{D_{12}}{R_0} \quad (\text{Eq. 2.24})$$

In order to process the registered peak and calculate D_{12} , several different techniques can be used, but the main approaches for this calculation are the moments method, the fitting method and the previously described graphical method, that consists in applying Eq. 2.23.

Alternatively, in the moments method, D_{12} is calculated through a simplification that results from the combination of Eq. 2.14 and Eq. 2.25. The equation that results from this simplification, Eq. 2.26, is valid if $D_{12} \bar{t} R_0^{-2} > 10$ and can be used since the error associated to it is no more than ± 1 %.

$$\sigma^2 = \frac{2D\bar{t}}{\bar{u}^2} \quad (\text{Eq. 2.25})$$

$$D_{12} = \frac{R_0^2 \bar{t}}{24\sigma^2} \quad (\text{Eq. 2.26})$$

In the equations shown above, the use of \bar{t} instead of t assumes that there is no dispersion of the pulse while it passes through the detection system. Additionally, \bar{t} and σ^2 can be calculated using the zeroth, first and second temporal moments of the concentration distribution curve. These temporal moments are described by [58]:

$$S = \int_0^{\infty} \bar{c}(t) dt \quad (\text{Eq. 2.27})$$

$$\bar{t} = \frac{1}{S} \int_0^{\infty} t \bar{c}(t) dt \quad (\text{Eq. 2.28})$$

$$\sigma^2 = \frac{1}{S} \int_0^{\infty} (t - \bar{t})^2 \bar{c}(t) dt \quad (\text{Eq. 2.29})$$

At last, in the fitting method, D_{12} is calculated by non-linear fitting of the obtained peak, by minimizing the square root of the mean square error, ε , which is defined by:

$$\varepsilon = 100 \times \sqrt{\frac{\int_{t_1}^{t_2} [\bar{c}(t) - c^{exp}(t)]^2 dt}{\int_{t_1}^{t_2} [c^{exp}(t)]^2 dt}} \quad (\text{Eq. 2.30})$$

In the previous equation, c^{exp} is the experimentally measured concentration profile at column end, \bar{c} is the calculated concentration profile, given by Eq. 2.31 (after substituting $z = L$ in Eq. 2.13), and t_1 and t_2 are the interval limits for the chosen fitting period. The fitting period is selected so the measured response curve is higher than 10 % of the peak height and $t_1 < t_2$ [36,59,60].

$$\bar{c} = \frac{m}{\pi R_0^2} \cdot \frac{1}{2\sqrt{\pi D t}} \exp\left[-\frac{(L - \bar{u}t)^2}{4Dt}\right] \quad (\text{Eq. 2.31})$$

According to Funazukuri *et al*, for values of ε lower than 1 % this method performs a good fit and for values lower than 2 % or 3 %, the fit is also acceptable [36,56,61]. Besides that, if the peak has asymmetric factors higher than 1.2 or 1.3 they should be rejected.

After obtaining the values of \bar{t} and σ^2 that correspond to a good fit, the value of D_{12} is calculated using Eq. 2.26 [62].

Funazukuri *et al*. also stated that the value of D_{12} obtained through the fitting method is more accurate when compared with the moments method. This happens because the

moments method overestimates the errors related to the frontal and tailing portions of the response curve in the higher moments [36].

Later in 2010, Lin and Tavlarides [63] concluded that the linearity of the UV detector is crucial to the accuracy of the measurements performed by the CPB method. It was found the best linearity results correspond to the maximum diffusion coefficients, and for that reason, the wavelength which gives maximum diffusion coefficients should be selected for dispersion peak detection [64]. In this thesis, similarly to other researchers [36,59,65], a distinct approach is adopted (see Chapters 5.2 and 5.3).

The CPB method is an attractive technique to measure diffusion coefficients since it is precise, allows to obtain the experimental data in a short time [35] and requires very small quantities of solute [66]. On the other hand, the injection of solutes is very restricted, since viscous liquids or solid solutes may adsorb on the column walls and cause difficulties in the system [67]. The biggest disadvantage of the chromatographic method is the fact that only diffusion coefficients at infinite dilution are measured, since the injected solute quantity do not exceed 1 μL [49].

In order to overcome the difficulties related to the injection of solids or viscous solutes, two other impulse responsive methods were developed: the chromatographic impulse response (CIR) technique and the modified Taylor-Aris technique [36].

2.2 Chromatographic impulse response (CIR) technique

The chromatographic impulse response (CIR) technique is a widely used method to measure solubilities and retention factors for gases, liquids and supercritical fluids, which was firstly used by Funazukuri *et al.* [36] and is based on the work of Lai and Tan. In this technique, a diffusion column coated with poly(ethylene glycol) or other polymers film is used, instead of the regular empty column used in the CPB method [38,65,68]. Due to this alteration, the problems of using viscous liquids or solid solutes can be overcome, since their solubility in the carrier solvent can be ensured by adding an organic solvent. This addition is only possible because the solute and the added organic solvent are chromatographically separated in the polymer-coated column, making it easy to eliminate the effect of the solvent,

as shown in Figure 2.3. Besides that, the choice of the polymer coating helps to minimize the distortion or tailing of the response curves for polar compounds [59].

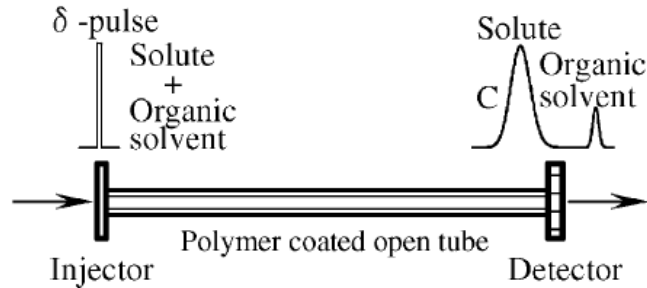


Figure 2.3- Schematic diagram of the CIR technique [36].

This separation occurs due to the different retention factors, k , or capacity factors, that are defined as the ratio of a compound in the polymer phase to that in the fluid phase.

Practically, k values are calculated by Eq. 2.32, which uses the measured peak retention times. In this equation, t_{tr} and t_0 are the retention times of the tracer and the inert species ($k = 0$), respectively.

$$k = \frac{t_{tr} - t_0}{t_0} \quad (\text{Eq. 2.32})$$

As can be seen in Figure 2.3, the CIR technique is very similar to the CPB method, being different only on the type of column used. In fact, the dispersion of the injected pulse in the CIR technique is mathematically described by the same equation presented for the CPB method, Eq. 2.1. However, the boundary first condition is different [36]:

$$\text{at } r = R_0, k \frac{\partial c}{\partial t} = -\frac{2D_{12}}{R_0} \cdot \frac{\partial c}{\partial r} \quad (\text{Eq. 2.33})$$

$$\text{at } r = 0, \frac{\partial c}{\partial r} = 0 \quad (\text{Eq. 2.34})$$

$$\text{at } z = \pm\infty, c = 0 \quad (\text{Eq. 2.35})$$

where the retention factor, k , is assumed to be constant regardless of the axial position in the column and the time, but is affected by the temperature and pressure. It is also presumed that the adsorption isotherm is linear and the tracer component instantaneously reaches equilibrium between the fluid and the polymer layer on the wall [59].

Assuming the tracer component reaches the equilibrium on the wall at the exact same time of the injection ($t = 0$), the initial condition for the pulse input is given by Eq. 2.36.

$$\text{at } t = 0, \quad c = \frac{m}{\pi R_0^2} \frac{\delta(z)}{1+k} \quad (\text{Eq. 2.36})$$

Since the average concentration over cross sectional area of tubing is defined by Eq. 2.7 just as in the CPB method, Golay derived a gaussian like approximate solution from Eqs. 2.1, 2.33 and 2.34. This approximation is given by:

$$\frac{\partial \bar{c}}{\partial t} = a \frac{\partial^2 \bar{c}}{\partial z'^2} - b \frac{\partial^2 \bar{c}}{\partial z' \partial t} \quad (\text{Eq. 2.37})$$

where,

$$a = \frac{D_{12}}{1+k} + \frac{1+6k+11k^2}{1+k} \frac{R_0^2 U^2}{48D_{12}} \quad (\text{Eq. 2.38})$$

$$b = \frac{k(1+4k)}{1+k} \frac{R_0^2 U}{24D_{12}} \quad (\text{Eq. 2.39})$$

$$z' = z - Ut \quad (\text{Eq. 2.40})$$

$$U = \frac{\bar{u}}{1+k} \quad (\text{Eq. 2.41})$$

Under the general conditions of diffusion measurements for liquids and supercritical fluids, the second term of Eq. 2.37 can be set to zero, resulting in the simplification described by Eq. 2.42 and the new boundary conditions described by Eqs. 2.43 and 2.44 [59,68].

$$\frac{\partial \bar{c}}{\partial t} = a \frac{\partial^2 \bar{c}}{\partial z'^2} \quad (\text{Eq. 2.42})$$

$$\text{at } t = 0, \quad \bar{c} = \frac{m}{\pi R_0^2} \frac{\delta(z')}{1+k} \quad (\text{Eq. 2.43})$$

$$\text{at } z' = \pm\infty, \quad \bar{c} = 0 \quad (\text{Eq. 2.44})$$

By solving Eq. 2.42, it is obtained the gaussian like analytical solution for the CIR method with linear adsorption model. This solution is given by [36,59]:

$$\bar{c} = \frac{m}{\pi R_0^2} \cdot \frac{1}{(1+k)2\sqrt{\pi at}} \exp \left[-\frac{(z-Ut)^2}{4at} \right] \quad (\text{Eq. 2.45})$$

The experimental values of D_{12} and k can be determined by the same adjusting numerical methods discussed in Chapter 2.1 for the CPB method.

In the fitting method, the values of a and U are obtained by minimizing the square root of the mean square error, ε , described by Eq. 2.30.

By knowing the values of a and U and using Eqs. 2.41 and 2.46, the values of D_{12} and k are obtained. It is important to remember that just as in the CPB method, a good fit correspond to values of ε lower than 1 % [36,59,68].

$$D_{12} = \frac{\left[\frac{1 + 6k + 11k^2}{1 + k} \right] \left[\frac{R_0^2 U^2}{24a} \right]}{1 + \sqrt{1 - \left[\frac{1 + 6k + 11k^2 R_0^2 U^2}{(1 + k)^2 12a^2} \right]}} \quad (\text{Eq. 2.46})$$

On the other hand, in the moments method D_{12} and k are obtained by:

$$D_{12} = \frac{2\beta}{\alpha + \sqrt{(\alpha^2 + 4\beta)}} L\bar{u} \quad (\text{Eq. 2.47})$$

$$k = \frac{4 - 2\left(\frac{\sigma^2}{\bar{t}^2}\right)}{3 + \sqrt{\left[1 + 4\left(\frac{\sigma^2}{\bar{t}^2}\right)\right]}} \frac{\bar{u}\bar{t}}{L} - 1 \quad (\text{Eq. 2.48})$$

The values of \bar{t} , σ^2 , α and β are obtained through the equations shown below [68]:

$$\bar{t} = \frac{\int_0^\infty t c^{exp} dt}{\int_0^\infty c^{exp} dt} \quad (\text{Eq. 2.49})$$

$$\sigma^2 = \frac{\int_0^\infty (t - \bar{t})^2 c^{exp} dt}{\int_0^\infty c^{exp} dt} \quad (\text{Eq. 2.50})$$

$$\alpha = \frac{2\left(\frac{\sigma^2}{\bar{t}^2}\right) - 1 + \sqrt{1 + 4\left(\frac{\sigma^2}{\bar{t}^2}\right)}}{8 - 4\left(\frac{\sigma^2}{\bar{t}^2}\right)} \quad (\text{Eq. 2.51})$$

$$\beta = \frac{1 + 6k + 11k^2 R_0^2}{(1 + k)^2 48L^2} \quad (\text{Eq. 2.52})$$

2.3 Modified Taylor-Aris technique

As previously mentioned, the modified Taylor-Aris technique was developed to overcome difficulties of solute injection into the diffusion column [36].

In this method, a polymer-coated column is placed before the diffusion column to separate the solute from the organic solvent. This particular column disposition, presented in Figure 2.4, makes this method suitable to measure diffusivities of volatile compounds.

To calculate the binary diffusion coefficients, the solute concentration is measured at the inlet and the outlet of the uncoated column in order to determine the difference in variance at these two points [65].

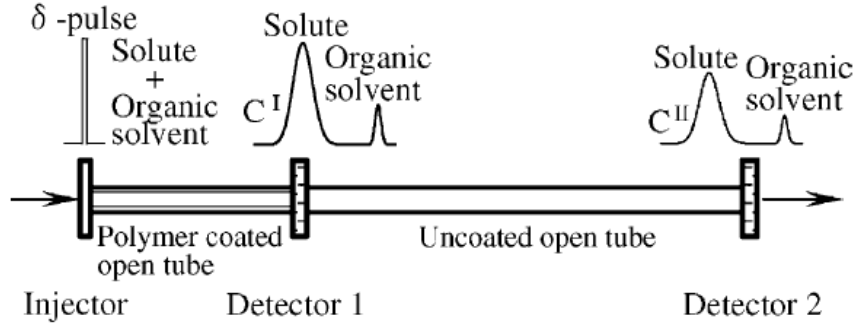


Figure 2.4- Schematic diagram of the modified Taylor-Aris technique [36].

As in the CPB method, the cross-sectional average concentration of an injected tracer species with asymptotic behavior is described by Eqs. 2.8 and 2.9. However, the boundary conditions are given by:

$$\text{at } t = 0, \bar{c} = 0 \quad (\text{Eq. 2.53})$$

$$\text{at } z = 0, \bar{c} = c^{exp I}(t) \quad (\text{Eq. 2.54})$$

Combining Eqs. 2.8, 2.9, 2.12, 2.53 and 2.54, one obtains:

$$\bar{c}^{II}(t) = \int_0^t c^{exp I}(\xi) f(t - \xi) d\xi \quad (\text{Eq. 2.55})$$

where D is given by Eq. 2.9 and $f(t)$ is given by Eq. 2.56. $f(t)$ is the Laplace inversion of the transfer function $F(s)$.

$$f(t) = \frac{L}{\sqrt{4\pi Dt^3}} \exp \left[-\frac{(L - \bar{u}t)^2}{4Dt} \right] \quad (\text{Eq. 2.56})$$

As shown in Eq. 2.57, $F(s)$ is the ratio of the Laplace transform of the output signal $c^{exp II}(t)$ to that of the input signal $c^{exp I}(t)$.

$$F(s) = \frac{\int_0^\infty c^{exp II}(t) e^{-st} dt}{\int_0^\infty c^{exp I}(t) e^{-st} dt} = \exp \left[\frac{L\bar{u} \left(1 - \sqrt{1 + 4 \left(\frac{Ds}{\bar{u}^2} \right)} \right)}{2D} \right] \quad (\text{Eq. 2.57})$$

The value of D_{12} is determined by minimizing the square root of the mean square error, using Eq. 2.30, as in the CPB method, but instead of using $c^{exp}(t)$ and $\bar{c}(t)$ it is used $c^{exp II}(t)$ and $\bar{c}^{II}(t)$, respectively [36,65].

Chapter 3

Modeling tracer diffusion coefficients

The transport properties play a big role in the design and optimization of rate-controlled extraction and separation processes in general, either in industry or in the research field. Thus, the capacity of having reliable values of diffusivity for various systems is of extreme importance, and, therefore, its rigorous determination using literature models is a great asset to describe and know better the behavior of dense fluids and supercritical fluids.

In the current work, several models were selected to estimate and correlate the tracer diffusivities, which are used later for comparison with the experimental data. However, it is important to note that only a small fraction of the existing models were selected since there are innumerable, as shown on the review of Medina [64]. Each model has their own limitations and applicability restrictions [69-71].

The selected models can be grouped in five different categories: models based on the free volume theory; models based on the hydrodynamic theory; models based on the rough hard sphere theory; hybrid models; empirical and semi-empirical correlations.

The models performance was assessed by the average absolute relative deviation, AARD, which is defined by [49]:

$$AARD = \frac{100}{NDP} \sum_{i=1}^{NDP} \left| \frac{D_{12}^{calc} - D_{12}^{exp}}{D_{12}^{exp}} \right|_i \quad (\text{Eq. 3.1})$$

3.1 Models based on the free volume theory

Free volume theories have a high interest in the calculation of transport properties, namely the self-diffusion coefficient (D_{11}), the viscosity (μ) and the thermal conductivity (κ) [49]. These theories state that such properties depend on the relative expansion from an intrinsic molar volume (V_{in}) [72]. These theories are very important due to the following reasons [49]:

- i. Their equations are simple and involve a small number of parameters (usually between two and four).
- ii. The parameters involved have, almost always, a precise physical meaning.
- iii. Their equations can be used over wide ranges of temperature and pressure.
- iv. The main theories have a very solid theoretical background since they are based on statistical mechanics.
- v. They can be easily extended to multicomponent systems.

One of the major free volume equations is the Dymond-Hildebrand-Batschinski (DHB), which is frequently used to describe non-polar compounds with negligible attractive forces at moderate densities [72].

Dymond-Hildebrand-Batschinski (DHB) correlation

Based on the work of Batschinski for real liquids, Hildebrand studied self-diffusivities and suggested a dependency between diffusion coefficients and the free molar volume [73].

In 1974, Dymond found the computer results that he obtained for hard sphere systems could be fitted into an equation almost similar to the one proposed and reestablished by Batschinski and Hildebrand, respectively. He ended up proposing Eq. 3.2, which includes dependency on the square root of the temperature [74,75].

$$D_{12} = B_{DHB} \sqrt{T} (V_i - V_D) \quad (\text{Eq. 3.2})$$

In Eq. 3.2, V_i is the molar volume ($\text{cm}^3 \text{mol}^{-1}$) and V_D is the minimum molar volume for which no diffusion occurs ($\text{cm}^3 \text{mol}^{-1}$). This parameter varies from solvent to solvent and is also called maximum packing volume. T is the temperature (K) and B_{DHB} is a model parameter that depends on the system in study ($\text{cm}^{-1} \text{mol}^{-1} \text{s}^{-1} \text{K}^{-0.5}$) [75-77].

It is important to note that in some systems, the value of V_D may depend on the temperature. Simple relations, such as a linear dependency ($V_D = m_{V_D} T + b_{V_D}$), have been used in previous works to describe this behavior [72,78].

3.2 Models based on the hydrodynamic theory

The hydrodynamic theory considers the diffusion of large spherical molecules through a dilute solution. The basis of this theory is the relation of Nernst-Einstein, which is traduced in Eq. 3.3, and relates the diffusion coefficient (D_{12}) and the mobility (ν) of the diffusing

particles. The mobility of a particle can be expressed as, $u \cdot F^{-1}$, where u is the velocity of a particle subjected to the action of a force F [35,79,80].

$$D_{12} = \nu k_B T = \frac{u}{F} k_B T = \nu \frac{RT}{N_A} \quad (\text{Eq. 3.3})$$

where, k_B is the Boltzmann constant, R is the ideal gas constant and N_A is the Avogadro's number.

The hydrodynamic theory is the base of many models used to calculate the diffusion coefficient such as the Stokes-Einstein relation, the Wilke-Chang equation, the Scheibel equation, the Tyn-Calus equation, the Lai-Tan equation, the Reddy-Doraiswamy model and many others presented [64,70].

Stokes-Einstein relation

This relation, based on the hydrodynamic theory, considers that the diffusion occurs through a continuous medium of viscosity μ . Due to this consideration, the particle's mobility can be calculated using the Stokes law, as shown in Eq. 3.4, where R_p is the radius of the particle [81].

Combining Eqs. 3.3 and 3.4 it is obtained the Stokes-Einstein equation, presented in Eq. 3.5, which can be accurately applied to the diffusion of large unhydrated molecules in low molecular weight solvents or when the molar volume of the solute is greater than $500 \text{ cm}^3 \text{ mol}^{-1}$. This equation is only applicable to macroscopic systems [70,82].

$$\nu = \frac{1}{6\pi R_p \mu_1} \quad (\text{Eq. 3.4})$$

$$D_{12} = \frac{k_B T}{6\pi R_p \mu_1} \quad (\text{Eq. 3.5})$$

Wilke-Chang equation

Despite being proposed in 1955, this equation still is one of the most widely used. It consists in an empirical modification of the Stokes-Einstein equation, introducing the molecular weight of the solvent (M_1) in g mol^{-1} , the molar volume of the solute at its normal boiling temperature (V_2) in $\text{cm}^3 \text{ mol}^{-1}$, and the association factor of the solvent (ϕ), which is dimensionless. Wilke-Chang equation is presented in Eq. 3.6.

If there is no experimental data available to obtain the value of V_2 , it can be used the Tyn and Calus method, shown below as Eq. 3.7, to estimate it [69,70].

$$D_{12} = \frac{7.4 \times 10^{-8} (\phi M_1)^{1/2} T}{\mu_1 V_2^{0.6}} \quad (\text{Eq. 3.6})$$

$$V_2 = 0.285 \times V_c^{1.048} \quad (\text{Eq. 3.7})$$

Wilke and Chang recommend that ϕ should be 2.6 if the solvent is water, 1.9 if the solvent is methanol, 1.5 for ethanol, 1.2 for propanol and 1 for other solvents. Although the original value of ϕ stated for water was 2.6, when the original data were reanalyzed, the empirical best fit was 2.26 [70,82].

When it is not used only one solvent, but a mixture of many, Wilke-Chang equation can still be used, but μ_1 has to be replaced by the viscosity of the mixture and the ϕM_1 parameter is calculated by [82]:

$$\phi M_1 = \sum_{i=1}^N x_i \phi_i M_i \quad (\text{Eq. 3.8})$$

Scheibel equation

Scheibel's equation results from an attempt to generalize the correlation of Wilke-Chang involving the molar volumes of the solute and the solvent, V_2 and V_1 respectively. This equation, shown in Eq. 3.9, is only valid when the condition expressed in Eq. 3.10 is fulfilled [69,83,84].

$$D_{12} = 8.2 \times 10^{-8} \frac{T}{\mu_1} \frac{1 + \left(\frac{3V_1}{V_2}\right)^{2/3}}{V_2^{1/3}} \quad (\text{Eq. 3.9})$$

$$2 \leq \frac{V_2}{V_1} \leq 3 \quad (\text{Eq. 3.10})$$

In order to use Eq. 3.9 properly, the temperature (T) must be in K, the viscosity (μ_1) must be in cP, the molar volumes (V_i) must be in $\text{cm}^3 \text{mol}^{-1}$ and the diffusion coefficient is calculated in $\text{cm}^2 \text{s}^{-1}$

Tyn-Calus equation

Also based on the hydrodynamic theory and the Stokes-Einstein relation, Tyn and Calus proposed an equation to estimate the binary diffusion coefficient that introduces the parachors of the solute and solvent. This equation is given by Eq. 3.11.

Parachor is a parameter related with the compound liquid surface tension and it is calculated by Eq. 3.12.

$$D_{12} = 8.93 \times 10^{-8} \left(\frac{V_2}{V_1^2} \right)^{1/6} \left(\frac{P_1}{P_2} \right)^{0.6} \frac{T}{\mu_1} \quad (\text{Eq. 3.11})$$

$$P_i = V_i \gamma_i^{0.25} \quad (\text{Eq. 3.12})$$

where P_i is the parachor of species i in $\text{cm}^{3.25} \text{g}^{0.25} \text{s}^{-0.5} \text{mol}^{-1}$, V_i is the molar volume in $\text{cm}^3 \text{mol}^{-1}$, γ_i is the surface tension in g cm s^{-2} and μ_1 is solvent viscosity in cP.

In order to estimate the surface tension, Eq. 3.13 can be used. In this equation p_c is the critical pressure in bar, T_c is the critical temperature in K, $T_{br} = T_b T_c^{-1}$, where T_b is the temperature at the atmospheric boiling point in K, and α_c is calculated by Eq. 3.14.

$$\gamma = p_c^{2/3} T_c^{1/3} (0.132 \alpha_c - 0.279) (1 - T_{br})^{11/9} \quad (\text{Eq. 3.13})$$

$$\alpha_c = 0.9076 \left[1 + \frac{T_{br} \ln \left(\frac{p_c}{1.013} \right)}{1 - T_{br}} \right] \quad (\text{Eq. 3.14})$$

When using Eq. 3.11, Tyn and Calus noted that this equation should not be used for solvents that have a viscosity above 20 cP.

For organic liquids is possible to have a simplified version of Eq. 3.11 after combining it with Eq. 3.12. The combined equation is presented below in Eq. 3.15 and the simplified version is Eq. 3.16. This simplification results from the fact that most organic liquids at T_b have similar surface tensions, making it possible to approximate its ratio to one [70,82].

$$D_{12} = 8.93 \times 10^{-8} \frac{V_1^{0.267} T}{V_2^{0.433} \mu_1} \left(\frac{\gamma_1}{\gamma_2} \right)^{0.15} \quad (\text{Eq. 3.15})$$

$$D_{12} = 8.93 \times 10^{-8} \frac{V_1^{0.267} T}{V_2^{0.433} \mu_1} \quad (\text{Eq. 3.16})$$

Lai-Tan equation

Based on the Wilke-Chang model, Lai-Tan proposed an empirical modified equation that takes into account the nonlinear variation of D_{12} with μ_1^{-1} . This equation, specially developed to supercritical carbon dioxide systems, is given by:

$$D_{12} = 2.50 \times 10^{-7} \frac{T \sqrt{M_1}}{(10 \mu_1)^{0.688} V_{c,2}^{0.284}} \quad (\text{Eq. 3.17})$$

where M_1 is the molar mass of the solvent in g mol^{-1} , $V_{c,2}$ is the critical molar volume of the solute in $\text{cm}^3 \text{mol}^{-1}$ and the viscosity (μ_1) is in cP [38].

Reddy-Doraiswamy model

In an attempt to generalize the Wilke-Chang equation, by removing the association factor of the solvent (ϕ), Reddy and Doraiswamy developed Eq. 3.18 [62,85].

$$D_{12} = \beta \frac{T\sqrt{M_1}}{\mu_1(V_1V_2)^{1/3}} \quad (\text{Eq. 3.18})$$

The value of β is determined by the following conditions:

$$\text{if } \frac{V_1}{V_2} \leq 1.5 \quad \beta = 10 \times 10^{-8} \quad (\text{Eq. 3.19})$$

$$\text{if } \frac{V_1}{V_2} > 1.5 \quad \beta = 8.5 \times 10^{-8} \quad (\text{Eq. 3.20})$$

3.3 Models based on the rough hard sphere theory

So far, the discussed models are based on theories that are limited to systems that have much larger solute molecules than the molecules of the solvent or to systems where the solvent densities are greater than the critical density. Besides that, those correlations were developed from empirical work. Since the pressures studied in this work are quite high, it is not easy to present a rigorous theoretical interpretation of the transport properties. This happens because the fluids are too dense, which result in many body interactions, and the pair potential energy functions are only known for simple molecules [72].

Since in dense fluids the repulsive molecular interactions have a big impact on their properties, Enskog considered the particles as rigid spheres and proposed a new kinetic theory. The only assumptions that he considered were that:

- i. Only binary collisions occur between molecules.
- ii. The velocities of the colliding particles are uncorrelated and independent of the position.

Due to computer simulation, since 1970, the theory of Enskog for self-diffusivity, viscosity and thermal conductivity for hard sphere fluids has suffered several corrections in order to represent the dynamic behavior of real fluids [86,87]. The modified Enskog-Thorne theory for self- and binary diffusion coefficients, which results from an attempt to improve the Enskog theory, is the base of Catchpole-King correlation.

Catchpole-King correlation

Based on the modified Enskog-Thorne theory, Catchpole and King proposed a correlation to predict the self- and binary diffusion coefficients in near critical conditions, by correcting the self-diffusivity coefficient. According to them, the binary diffusion coefficient is calculated by:

$$D_{12} = 2^{2/3} D_{11} \frac{F}{X} \quad (\text{Eq. 3.21})$$

where X is a size to mass ratio parameter calculated by Eq. 3.22. The correction parameter F is calculated by Eq. 3.23 or Eq. 3.24 according to the system in study.

$$X = \frac{\left[1 + \left(\frac{V_{c,2}}{V_{c,1}} \right)^{1/3} \right]^2}{\sqrt{1 + \frac{M_1}{M_2}}} \quad (\text{Eq. 3.22})$$

For class one systems, where the solute is an aliphatic compound except ketones, F is calculated by:

$$F = 1.0 \pm 0.1, \quad 2 < X \quad (\text{Eq. 3.23})$$

For class two systems, where the solute is an aromatic compound, a ketone or carbon tetrachloride, F is calculated by:

$$F = X^{0.17} \pm 0.1, \quad 2 < X < 10 \quad (\text{Eq. 3.24})$$

The final correlation that Catchpole and King obtained is shown below in Eq. 3.25.

$$D_{12} = 5.152 \times 10^4 D_{c,11} T_r (\rho_{r,1}^{-2/3} - 0.4510) \frac{F}{X}, \quad 1 < \rho_{r,1} < 2.5 \quad (\text{Eq. 3.25})$$

In the previous equation, $D_{c,11}$ is the self-diffusion coefficient of the solvent at the critical point, that is calculated by Eq. 3.26, $T_r = T T_c^{-1}$ is the reduced temperature of the system, $\rho_{r,1}$ is the reduced density of the solvent. The calculated value of D_{12} is in $\text{cm}^2 \text{s}^{-1}$ [37,82,88].

$$D_{c,11} = \frac{4.300 \times 10^{-7} \sqrt{M} T_c^{0.75}}{\sum V_d^{2/3} \rho_c} \quad (\text{Eq. 3.26})$$

The previous equation was obtained from a modified empirical correlation developed by Fuller, Schettler and Gidding. In Eq. 3.26, M is the molar mass in g mol^{-1} , T_c is the critical temperature in K, ρ_c is the critical density of the compound in kg m^{-3} and V_d are the atomic diffusion volumes, and can be found in the literature [70].

3.4 Hybrid models

In order to have a better representation of the behavior of real dense fluids, hybrid models were developed. These models consider, at the same time, the free volume available to diffusion and the activation energy involved due to particles interactions.

Predictive model TLSM

The Tracer Liu-Silva-Macedo (TLSM) is a predictive model (zero parameters) that has its origin in the Liu-Silva-Macedo (LSM) model for the prediction of self-diffusion coefficients [76]. This model allows the estimation of D_{12} at temperature T and solvent number density $\rho_{n,1}$ by only knowing three input parameters per molecule: the molecular weight, the Lennard-Jones (LJ) diameter and the LJ energy [89].

The TLSM model, which is represented by Eq. 3.27, is a hybrid model since it presents an exponential term of free volume (the reduced density of the solvent) and a term involving the activation energy (the reduced temperature).

$$D_{12} = \frac{21.16}{\rho_{n,1}\sigma_{12,eff}^2} \left(\frac{1000RT}{2M_{12}} \right)^{1/2} \exp \left(-\frac{0.75\rho_{rn,1}^*}{1.2588 - \rho_{rn,1}^*} - \frac{0.27862}{T_{r,12}^*} \right) \quad (\text{Eq. 3.27})$$

Here, D_{12} is calculated in $\text{cm}^2 \text{s}^{-1}$, $\rho_{n,1}$ is the solvent number density that is calculated by Eq. 3.28 in cm^{-3} , $\sigma_{12,eff}$ is the effective hard sphere diameter in cm that is calculated by Eq. 3.29, R is the ideal gas constant ($8.3144 \text{ J mol}^{-1} \text{ K}^{-1}$), T is the temperature in K, M_{12} is the reduced molar mass of the system that is calculated by Eq. 3.30 in g mol^{-1} , $\rho_{rn,1}^*$ is the reduced number density of the solvent that is calculated by Eq. 3.31 and $T_{r,12}^*$ is the reduced temperature that is calculated by Eq. 3.32.

$$\rho_{n,1} = \rho_1 \frac{N_A}{M_1} \quad (\text{Eq. 3.28})$$

$$\sigma_{i,eff} = \sigma_{i,LJ} 2^{1/6} [1 + \sqrt{1.3299 T_{r,i}^*}]^{-1/6}, \quad i = 1 \text{ or } 12 \quad (\text{Eq. 3.29})$$

$$M_{12} = \frac{M_1 M_2}{M_1 + M_2} \quad (\text{Eq. 3.30})$$

$$\rho_{rn,1}^* = \rho_{n,1} \sigma_{1,eff}^3 \quad (\text{Eq. 3.31})$$

$$T_{r,i}^* = \frac{T}{\varepsilon_{i,LJ}/k_B} \quad (\text{Eq. 3.32})$$

The Lennard-Jones parameters necessary in Eq. 3.29 and Eq. 3.32, can be calculated by Eq. 3.33 and Eq. 3.34.

$$\sigma_{12,LJ} = \frac{\sigma_{1,LJ} + \sigma_{2,LJ}}{2} \quad (\text{Eq. 3.33})$$

$$\frac{\varepsilon_{12,LJ}}{k_B} = \frac{\sqrt{\sigma_{1,LJ}^3 \frac{\varepsilon_{1,LJ}}{k_B} \times \sigma_{2,LJ}^3 \frac{\varepsilon_{2,LJ}}{k_B}}}{\sigma_{12,LJ}^3} \quad (\text{Eq. 3.34})$$

Since the LJ energies and diameters are often unknown for several compounds, these values can be estimated by Eq. 3.35 and Eq. 3.36 or Eq. 3.37, respectively.

$$\frac{\varepsilon_{i,LJ}}{k_B} (K) = 0.774T_c, \quad i = 1,2 \quad (\text{Eq. 3.35})$$

$$\sigma_{i,LJ}^3 (\text{\AA}^3) = 0.17791 + 11.779 \left(\frac{T_c}{p_c} \right) - 0.049029 \left(\frac{T_c}{p_c} \right)^2, \quad \text{for } \frac{T_c}{p_c} \leq 100 \quad (\text{Eq. 3.36})$$

$$\sigma_{i,LJ} (\text{\AA}) = 0.809V_c^{1/3}, \quad \text{for } \frac{T_c}{p_c} > 100 \quad (\text{Eq. 3.37})$$

It is important to note that, since this model is based on the LSM one, it cannot be successful applied to hydrogen bonding solvents like water or alcohols. The LSM equation is not applicable in these cases because, in what concerns to molecular interactions, it only considers van der Waals forces, which are much weaker than the ones that exist in hydrogen bonding solvents [72,76,89].

TLSM_d correlation (one parameter)

From the TLSM model it is possible to generate a one parameter correlation by inserting an interaction constant $k_{12,d}$ into the diameter combining rule. This constant is an adjustable parameter of the model. Thus, the binary LJ parameters are given by [76]:

$$\frac{\varepsilon_{12,LJ}}{k_B} = \frac{8 \sqrt{\sigma_{1,LJ}^3 \frac{\varepsilon_{1,LJ}}{k_B} \times \sigma_{2,LJ}^3 \frac{\varepsilon_{2,LJ}}{k_B}}}{(\sigma_{1,LJ} + \sigma_{2,LJ})^3} \quad (\text{Eq. 3.38})$$

$$\sigma_{12,LJ} = (1 - k_{12,d}) \frac{\sigma_{1,LJ} + \sigma_{2,LJ}}{2} \quad (\text{Eq. 3.39})$$

Using this model, D_{12} can be predicted with good accuracy, since there is a decrease of AARD from 15.71 % (for TLSM model) to 3.89 % (for TLSM_d model) showed by Magalhães *et al* [89] for a database of 5279 experimental points from 296 binary systems. Many values of the binary interaction constant $k_{12,d}$ are already tabled for various binary systems [71,89].

3.5 Empirical and semi-empirical correlations of Magalhães *et al.*

Magalhães *et al.* proposed several simple but very accurate, empirical and semi-empirical correlations, which express the diffusion coefficient as a dependency on the temperature, viscosity and density. These correlations are applicable over wide ranges of temperature and density, for systems composed of polar and non-polar, symmetrical and asymmetrical, small and large, light and heavy molecules without exception. They can be divided in four groups:

- i. Group 1, represented by Eq. 3.40, relates the diffusion coefficient with the temperature and the solvent viscosity.

$$\ln\left(\frac{D_{12}}{T}\right) = a_3 \ln \mu_1 + b_3 \quad (\text{Eq. 3.40})$$

- ii. Group 2, represented by Eq. 3.41, relates the diffusion coefficient only with the solvent viscosity.

$$D_{12} = a_5 \frac{1}{\mu_1} + b_5 \quad (\text{Eq. 3.41})$$

- iii. Group 3, represented by Eq. 3.42, relates the diffusion coefficient with the temperature and the solvent density.

$$\frac{D_{12}}{T} = a_7 \rho_1 + b_7 \quad (\text{Eq. 3.42})$$

- iv. Group 4, represented by Eq. 3.43, relates the diffusion coefficient with the temperature, the solvent density and the solvent viscosity.

$$\frac{D_{12}}{T} = a_9 \rho_1 + \frac{b_9}{\mu_1} \quad (\text{Eq. 3.43})$$

In all of these correlations, the temperature is in K, the solvent viscosity is in cP, the solvent density is in g cm⁻³ and D_{12} is calculated in cm² s⁻¹. The values of a_i and b_i represent the adjusted parameters of the equations [90].

Chapter 4

Experimental section

In this chapter are presented the experimental setup and chemical compounds used in the present work, the followed procedure and the conditions the measurements took place. It is also described the models used to estimate the density and viscosity of the solvents, that are later necessary to model the obtained data.

4.1 Equipment and procedure

As previously mentioned, in the current work, the technique used to measure the D_{12} was the CPB method [35-38]. A schematic representation of the utilized equipment is shown in Figure 4.1. Although in this work only ethanol and ethyl acetate have been used as solvents, the equipment is adapted to perform measurements with supercritical carbon dioxide (SC-CO₂).

The equipment includes two syringe pumps (2 and 4), that pump the solvents at constant flow rate from the reservoirs (1) and (5). The pumps are the Teledyne ISCO model 260D with a capacity of 266.06 cm³ for CO₂ and the Teledyne ISCO model 100 DM with a capacity of 102.97 cm³ for liquid solvent (ethanol or ethyl acetate). The CO₂ pump is coupled with a Julabo F12 thermostatic bath (3) to ensure there are no temperature oscillations that could cause flow rate fluctuations when working with SC-CO₂.

The equipment also includes a stainless-steel column (7) placed inside a LSIS-B2V/IC 22 oven (Venticell, MMM Group) (9) to pre-heat the solvents. This column is connected to an open capillary column with poly(ether ether ketone) (PEEK) coating (8) that is followed by a UV-visible detector (10) (UV Detector 2500, Knauer). The characteristics of the PEEK column are shown below in Table 4.1.

Additionally, there is a C74H-1674 injector (6) from Valco Instruments Co. Inc. used to inject the small pulses of solutes (0.1 μL) and a Jasco BP-2080 back pressure regulator (12) (BPR) to control the pressure inside the column. Coupled with the above-mentioned equipment, is a computer (11) with software that allows the acquisition of the absorbance data measured with the UV-visible detector.

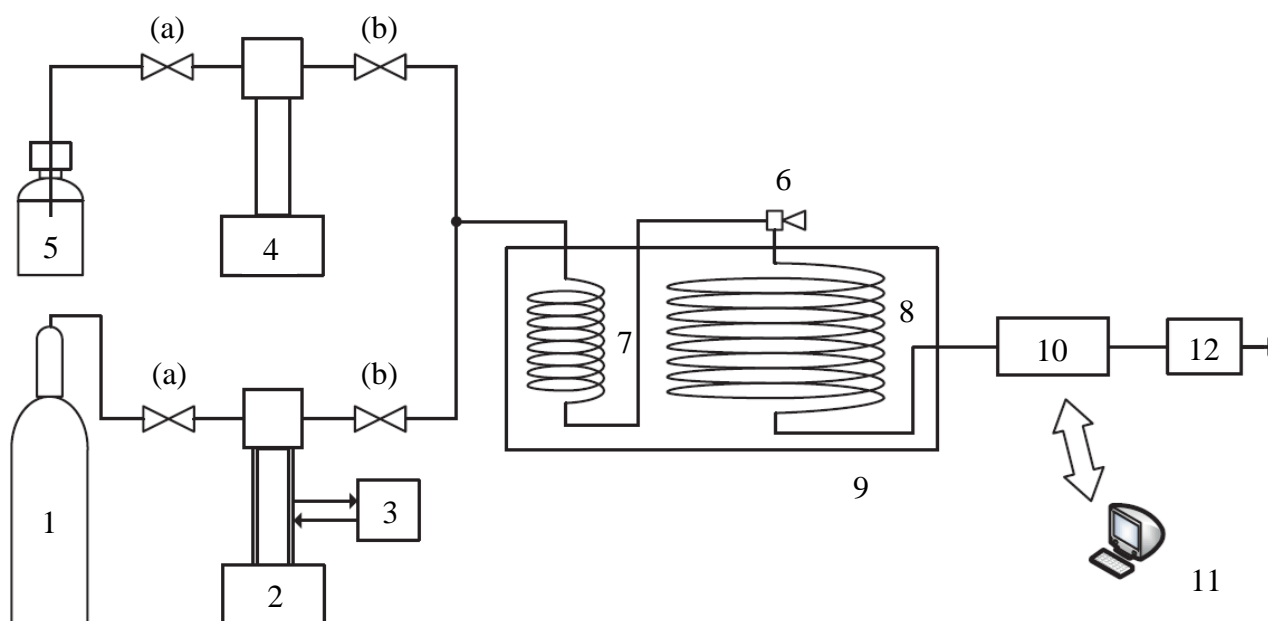


Figure 4.1- Schematic representation of the equipment used to perform the measurements of the D_{12} . (1) CO₂ cylinder, (2) CO₂ syringe pump, (3) thermostatic bath, (4) ethanol or ethyl acetate syringe pump, (5) ethanol or ethyl acetate reservoir, (6) injector, (7) pre-heating column, (8) diffusion column (with PEEK coating), (9) oven, (10) UV-visible detector, (11) computer with data acquisition software, (12) back pressure regulator – BPR, (a) on/off valves and (b) non return check valves.

Table 4.1- Characteristics of the diffusion column used in the experimental work.

Description	Diffusion column
Coating	Poly(ether ether ketone) (PEEK)
Length (cm)	1118.2
Internal radius (cm)	0.0261
Coiling radius (cm)	15.0

To ensure that the data of the measurements in pressurized ethanol or ethyl acetate are trustworthy, the procedure, which is described below, was followed carefully.

Firstly, it is necessary to turn on the oven, the UV-visible detector and the BPR, setting the desired operating conditions of temperature and pressure. The UV-visible detector has

to be set in the proper wavelength according to the system in use. This wavelength had to be previously studied.

After that, it is necessary to turn on the syringe pump that is connected to the reservoir of ethanol or ethyl acetate and do its refill. Once the syringe pump is full, it should be guaranteed that both in and out solvent valves are closed and the system should be pressurized up to the desired pressure. When the diffusion column reaches the desired pressure, it is time to insert in the syringe pump the desired flow rate to the operation, which in the current work was $0.150 \text{ mL min}^{-1}$.

Since the correct operability of the experimental equipment is very important to ensure the measured data are reliable, every time the equipment is started for one operating condition, the whole system has to stabilize for 1-2 hours, to ensure a steady-state operation of all components of the equipment. This guarantees that the temperature, the pressure, the flow rate and the absorbance signal (chromatogram baseline) are stable.

After the whole equipment has stabilized, it is finally possible to insert the solute in the diffusion column using the injector. It is important that the solute is injected quickly into the system to ensure that it is introduced as a pulse.

At last, it is only necessary to use the software present in the computer to register the absorbance data that is measured with the UV-visible detector and proceed to the treatment of the data.

4.2 Solutes and measurement conditions

The measurement of the diffusion coefficients of lycopene in ethanol and astaxanthin in ethyl acetate took place at 303.15, 313.15, 323.15 and 333.15 K, and at pressures of 1, 50 and 100 bar, at a wavelength of 255 nm for lycopene and 460 nm for astaxanthin. The selection of these wavelengths is further discussed in Chapters 5.2 and 5.3, respectively. It is also important to note that these solvents were chosen according to their solvent power and availability for industrial extractions [91,92].

The lycopene (CAS number 502-65-8) with purity of 85.00 % (HPLC) was purchased from AKSci while the astaxanthin (CAS number 472-61-7) with purity of 99.00 % (HPLC) was purchased from Sigma-Aldrich.

Regarding the solvents, absolute ethanol (CAS number 64-17-5) with purity of 99.99 % was supplied by Fisher Chemical and the ethyl acetate (CAS number 141-78-6) with purity of 99.99 % was supplied by CARLO ERBA Reagents S.A.S. More information about these compounds and their properties can be found in Appendices A and B, respectively.

4.3 Properties of the solvents

In order to analyze the experimental diffusion coefficients and model them with literature equations, it was necessary to estimate the density and viscosity of the solvents. The models used for this purpose are described below.

Density of liquid ethanol

The density of ethanol was estimated using the Tait equation [93,94], which presents very accurate results for alcohols:

$$\frac{\rho - \rho_0}{\rho} = 0.202 \times \log\left(\frac{B + p}{B + p_0}\right) \quad (\text{Eq. 4.1})$$

where, ρ and ρ_0 are densities (in g mL⁻¹) at pressures p and p_0 (in MPa). The parameter B is calculated by Eq. 4.2, where the temperature is used in K. In Eq. 4.3, C_n is the number of carbons of the molecule.

$$B = 520.23 - 1240 \times \frac{T}{T_c} + 827 \times \left(\frac{T}{T_c}\right)^2 - F \quad (\text{Eq. 4.2})$$

$$F = 0.015 \times C_n \times (1 + 11.5 \times C_n) \quad (\text{Eq. 4.3})$$

The density at atmospheric pressure (ρ_0) was calculated using Eykman correlation improved by Cano-Gómez *et al.* [95] (Eq. 4.4), where n_D is the refractive index and K is a characteristic constant.

$$\rho_0 = \frac{n_D^2 - 1}{n_D + 0.4} \times \frac{1}{K} \quad (\text{Eq. 4.4})$$

$$K = 0.72719 - 0.39294 \exp(C_n^{-0.89255} \times 0.47272) \quad (\text{Eq. 4.5})$$

$$n_D = a_0 + a_1 C_n^{a_2} + a_3 C_n + \frac{a_4}{C_n^{a_5}} + (a_6 + a_7 C_n^{0.5} + a_8 C_n^{0.75}) \times T \quad (\text{Eq. 4.6})$$

In Eq. 4.6, the temperature (T) is in °C and $a_0 = 1.87961$, $a_1 = -0.55029$, $a_2 = -0.11935$, $a_3 = -0.00161$, $a_4 = 0.01344$, $a_5 = 13.54426$, $a_6 = -0.00043235$, $a_7 = 0.00000954$ and $a_8 = 0.00000220$.

Viscosity of liquid ethanol

Based on the relation between viscosity and density proposed by Mamedov, Cano-Gómez *et al.* [96] developed a correlation to estimate the viscosity of primary alcohols at high pressures. This correlation is given by:

$$\frac{\mu}{\mu_0} = \left(\frac{\rho}{\rho_0}\right)^A \quad (\text{Eq. 4.7})$$

While the density (ρ) and the density at atmospheric pressure (ρ_0) were calculated by Eqs. 4.1 and 4.4, respectively, the parameter A was calculated by Eq. 4.8 and the viscosity at atmospheric pressure (μ_0) was calculated by Eq. 4.9 [97].

In Eq. 4.9, T is in K, μ_0 is in cP and $A = -6.4406$, $B = 1117.6$, $C = 0.013721$ and $D = -0.000015465$.

$$A = 10.4 + 0.00006 \times C_n^{3.5} - \frac{5}{C_n} \quad (\text{Eq. 4.8})$$

$$\log \mu_0 = A + \frac{B}{T} + C \times T + D \times T^2 \quad (\text{Eq. 4.9})$$

Density of liquid ethyl acetate

To estimate the density of ethyl acetate it was used the previously mentioned Tait equation [93,94], Eq. 4.1. However, the parameters involved in this equation, B and ρ_0 , are now calculated by Eqs. 4.10 and 4.11, respectively. The equation used to estimate the density at atmospheric pressure (ρ_0) is a modified form of the Rackett equation [97].

$$B = 494 - 1110 \times \frac{T}{T_c} + 672 \times \left(\frac{T}{T_c}\right)^2 - (C_n - 6) \quad (\text{Eq. 4.10})$$

$$\rho_0 = A \times B^{-\left(\frac{1-T}{T_c}\right)^n} \quad (\text{Eq. 4.11})$$

Here, the temperature is in K, ρ_0 is in g mL⁻¹ and $A = 0.30654$, $B = 0.25856$ and $n = 0.27800$.

Viscosity of liquid ethyl acetate

To estimate the viscosity of ethyl acetate it was used the previously mentioned correlation developed by Cano-Gómez *et al.* [96], Eq. 4.7.

The calculation of the viscosity of this compound is similar to the calculation of ethanol since the parameters necessary in Eq. 4.7 are also calculated by Eqs. 4.8 and 4.9. However, for ethyl acetate, the parameters involved in Eq. 4.9 are $A = -3.6861$, $B = 552.28$, $C = 0.0080018$ and $D = -0.000010439$.

Chapter 5

Results and discussion

In this chapter are presented and discussed the results of the experimental measurements of the diffusion coefficient of lycopene in ethanol and astaxanthin in ethyl acetate, as well as the results of the modeling. It is also shown the results that confirmed the validation of the equipment and experimental procedure of the D_{12} measurements.

5.1 Experimental equipment validation

Before measuring the diffusivity of lycopene and astaxanthin, it was necessary to ensure the experimental values registered by the equipment were reliable. With this purpose, the diffusion coefficient of gallic acid was measured at 1 and 100 bar and at 313.15 and 333.15 K in pressurized ethanol, and later compared with existing values in the literature [98]. The measurement conditions, namely the concentration of injected solute ($C = 1.76 \text{ mg mL}^{-1}$) and the detector wavelength ($\lambda = 280 \text{ nm}$), were the same that were used on the measurement of the literature values. In Table 5.1 are listed the experimental and published values of D_{12} of gallic acid, as well as the relative deviations between both values. These D_{12} values are also represented graphically in Figure 5.1 *versus* the temperature.

Table 5.1- Experimental and literature values of D_{12} of the gallic acid and their relative error.

Pressure (bar)	Temperature (K)	Measured $D_{12} \pm \Delta D_{12}$ ($10^{-5} \text{ cm}^2 \text{ s}^{-1}$)	Published $D_{12} \pm \Delta D_{12}$ [98] ($10^{-5} \text{ cm}^2 \text{ s}^{-1}$)	Relative error (%)
1	313.15	0.651 ± 0.008	0.624 ± 0.005	4.352
1	333.15	0.910 ± 0.028	0.905 ± 0.011	0.508
100	313.15	0.592 ± 0.002	0.592 ± 0.008	0.073
100	333.15	0.850 ± 0.006	0.846 ± 0.003	0.518

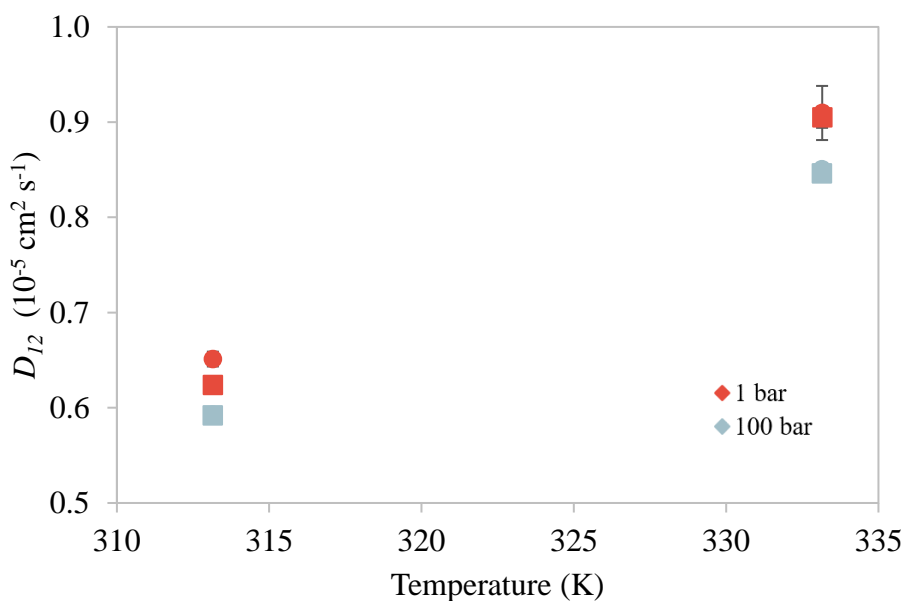


Figure 5.1- Comparison between the measured values (●) and the literature values [98] (■) of D_{12} of the gallic acid.

Taking a closer look at the Table 5.1 is possible to see that the maximum relative error between the measured value of D_{12} and the value presented in the literature is below 5 %, which proves the equipment and experimental procedure are accurate. This low relative error is traduced in almost overlapping dots in Figure 5.1, which present low variability, as is possible to see by the almost non-visible error bars. Each measured value in Table 5.1 and in Figure 5.1 is the average of seven individual injections.

Thus, through the obtained results, it is possible to conclude that the values of D_{12} obtained using the above-mentioned equipment and procedure are valid.

5.2 Tracer diffusivity of lycopene in ethanol

The measurements of the diffusion coefficient rely on the analysis of the experimental absorbance profiles recorded at the exit of the diffusion column by the UV-visible detector, and thus the selected wavelengths have extreme importance [63].

In order to select the optimal wavelength, which is the one that offers the best linearity results and the minimum experimental noise and error, several pulses of lycopene were injected for wavelengths in the range 205-265 nm. This range was selected by using UV-visible spectrophotometry to determine that this is the region where the maximum absorbance of lycopene is found, as can be seen in Appendix C. This preliminary study is

shown below in Figure 5.2. It is important to notice that due the low absorbance values registered for lycopene, the fitting interval of the peak was fixed in order to contain 40 % of the peak height instead of the usual 90 % mentioned in Chapter 2.1 (after Eq. 2.30), to reduce the interference of noise with the real absorbance peak.

Analyzing Figure 5.2 is possible to see a stable region that ranges from 235 to 255 nm that presents very small variations of D_{12} for the different wavelengths and low fitting errors. After a first analysis, more pulses were injected in this range of wavelengths to test the reproducibility of the results. The wavelength selected to perform the measurements was 255 nm, due its higher reproducibility over the others.

In Figure 5.2 is also possible to see a preliminar study of the relation between the injected concentration and the obtained D_{12} .

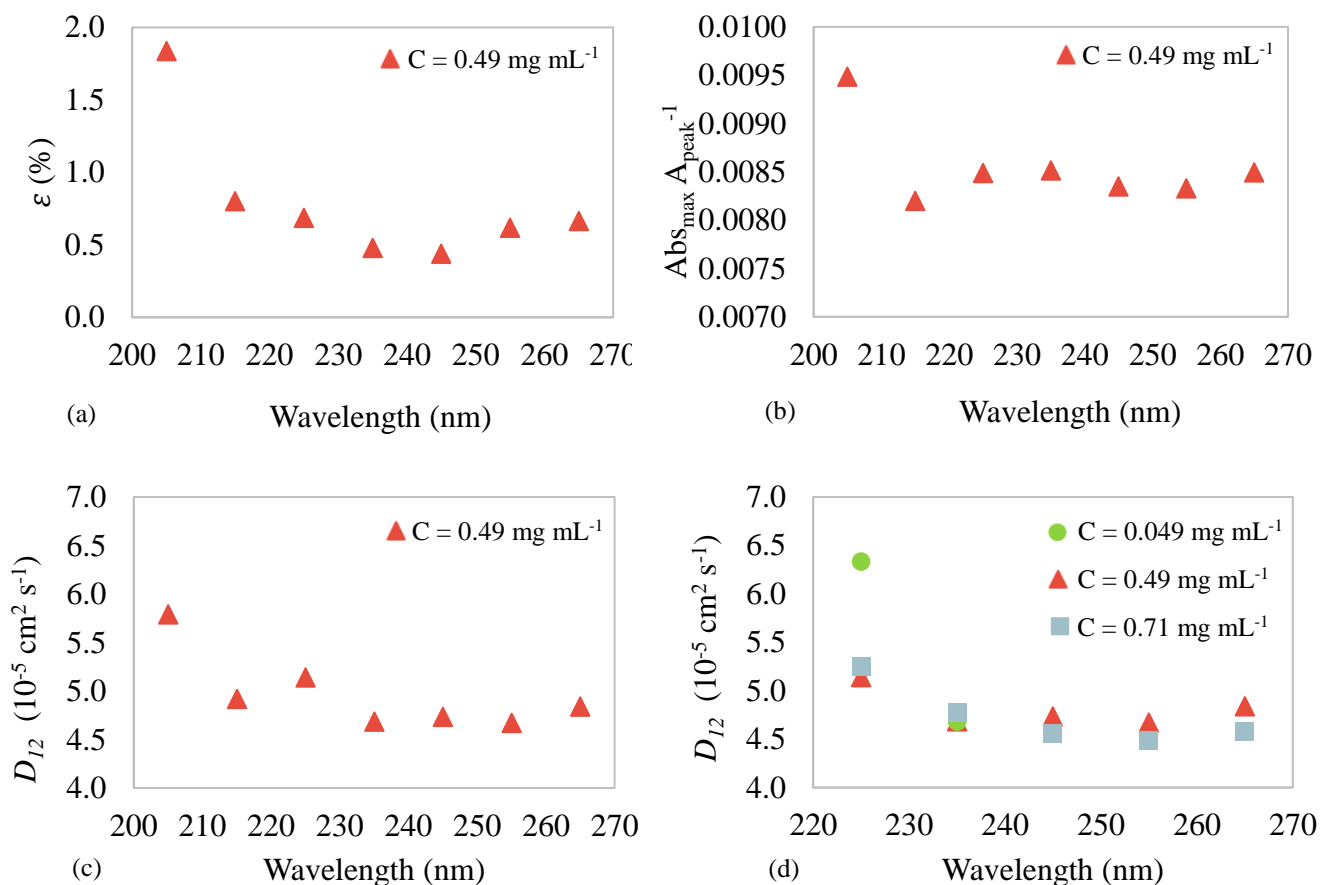


Figure 5.2- Determination of the optimal wavelength (λ) at 1 bar and 323.15 K, to study the diffusivity of lycopene in ethanol. (a) Root mean square error versus λ , (b) Ratio of maximum absorbance to peak area ($\text{Abs}_{\text{max}} A_{\text{peak}}^{-1}$) versus λ , (c) Preliminary D_{12} versus λ and (d) Preliminary D_{12} versus λ for $C = 0.049 \text{ mg mL}^{-1}$ (\bullet), $C = 0.49 \text{ mg mL}^{-1}$ (\blacktriangle) and $C = 0.71 \text{ mg mL}^{-1}$ (\blacksquare).

Three different concentrations were analyzed, $C = 0.049, 0.49$ and 0.71 mg mL^{-1} . Since there were no significant differences on the registered values of D_{12} for the various concentrations, it was decided to use $C = 0.49 \text{ mg mL}^{-1}$. This intermediate value ensures the peaks are high enough to be distinguished from the experimental noise (unlike $C = 0.049 \text{ mg mL}^{-1}$) and yet still not high enough to potentially cause obstructions inside the column (unlike $C = 0.71 \text{ mg mL}^{-1}$), since lycopene solubility in ethanol is quite low [99,100]. The amount of solute injected in the column was $9.127 \times 10^{-4} \text{ } \mu\text{mol}$, which ensures infinite dilution conditions inside the column [59,61,68].

A typical response curve obtained in this work for lycopene is shown in Figure 5.3, at 1 bar and 323.15 K. Similar curves were registered in all cases. The diffusivities obtained by the fitting method (Eqs. 2.9, 2.30 and 2.31) were almost identical to the ones obtained using the peak variance (Eqs. 2.15 and 2.23), due to the non-existence of tailing effects in the peak.

It is important to notice that the applicability of the CPB method was assured in every measurement, since the previously mentioned restrictions were fulfilled, namely: (i) low laminar flow rates (Re ranged from 2.19 to 3.92) caused by the low velocities of the solvent (\bar{u} ranged from 1.13 to 1.19 cm s^{-1}); (ii) very high longitudinal Peclet numbers (Pe_x varied between 1.91×10^8 and 3.90×10^8), meaning the axial dispersion can be neglected; (iii) the registered peaks were gaussian (since $D(\bar{u}L)^{-1} < 0.01$); (iv) the secondary flow effects due to the coiling of the column were also neglected (since $De\sqrt{Sc} < 10$); (v) the values of the square root of the mean square error were small (ϵ ranged from 0.40 to 1.58 %); (vi) the asymmetric factors of the peaks were close to one.

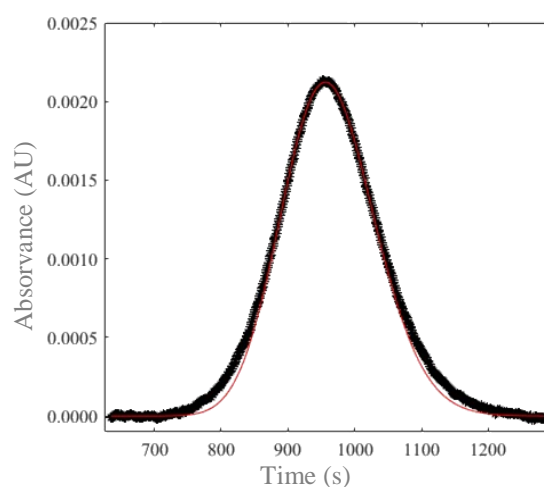


Figure 5.3- Experimental response curve (\times) and calculated curve ($-$) for lycopene in ethanol ($\lambda = 255 \text{ nm}$) at 1 bar and 323.15 K.

The obtained diffusivities for lycopene in ethanol varied between 0.374×10^{-5} and $0.668 \times 10^{-5} \text{ cm}^2 \text{ s}^{-1}$, for a temperature range of 303.15 to 333.15 K and a pressure range of 1 to 100 bar. These values are reported in Table 5.2 and plotted in Figure 5.4 *versus* the pressure.

Table 5.2- Experimental conditions, experimental D_{12} of lycopene in ethanol obtained through the CPB method and calculated density and viscosity of the solvent.

Temperature (K)	Pressure (bar)	$D_{12} \pm \Delta D_{12}$ ($10^{-5} \text{ cm}^2 \text{ s}^{-1}$)	Density (g cm^{-3})	Viscosity (cP)
303.15	1	0.374 ± 0.008	0.965	0.782
	50	0.366 ± 0.005	1.063	0.791
	100	0.345 ± 0.009	1.166	0.801
313.15	1	0.443 ± 0.005	0.810	0.773
	50	0.436 ± 0.017	0.899	0.783
	100	0.425 ± 0.009	0.991	0.793
323.15	1	0.535 ± 0.011	0.687	0.764
	50	0.505 ± 0.011	0.767	0.775
	100	0.501 ± 0.010	0.850	0.785
333.15	1	0.668 ± 0.010	0.587	0.756
	50	0.663 ± 0.005	0.659	0.767
	100	0.624 ± 0.004	0.735	0.777

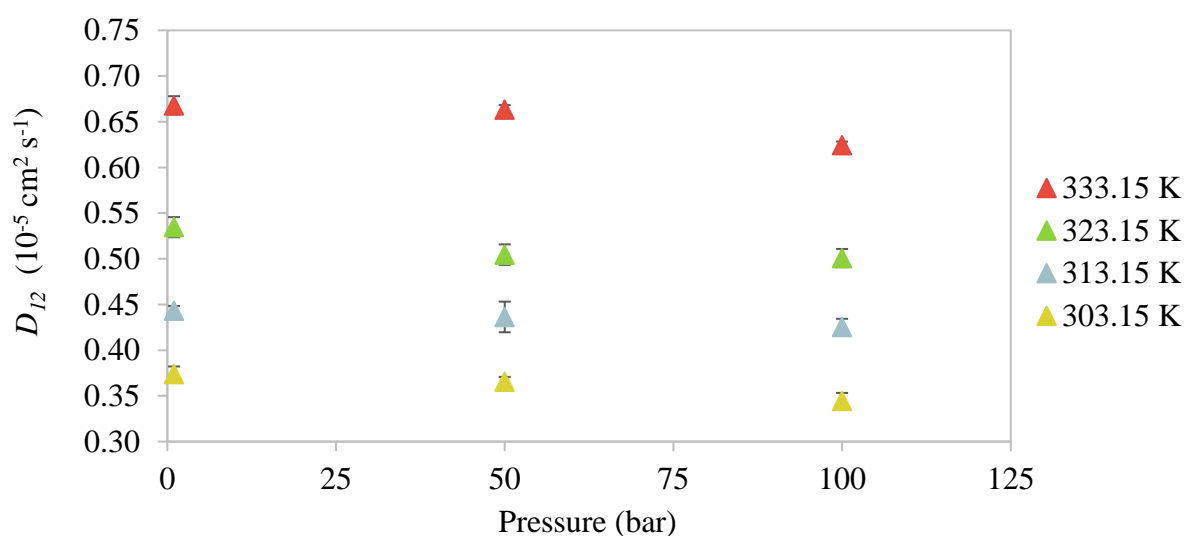


Figure 5.4- D_{12} of lycopene in ethanol as function of pressure for several temperatures.

Analysing the data presented in Table 5.2 and Figure 5.4 it is noticeable a clear pressure dependence of D_{12} at constant temperature. As expected, the D_{12} decreases as the pressure increases, which is in accordance with the free volume theories. An increase in pressure leads to higher densities, which in practice results in a more tightly packing of the solvent molecules. This packing reduces the free volume available for the molecules of solute to move as well as increases the energetic barrier that these molecules need to overcome in order to diffuse through the solvent [101,102]. The negative effect that the increase in density has on D_{12} , explained by free volume theories, is most evident in Figure 5.5

It is also possible to see in Figure 5.4 that under isobaric conditions an increase of temperature also increases the value of D_{12} . This rise of D_{12} is explained not only by the decrease of the density (which increases the free volume available), but also by the increase of the kinetic energy of the molecules of solute, which in this way move more easily [64]. These behaviors recorded under isothermal and isobaric conditions are consistent with results reported in other works [43,78,98,103].

It was also studied the hydrodynamic behavior of the system adopting the Stokes-Einstein coordinates. In Figure 5.6 are plotted the values of D_{12} versus $T\mu^{-1}$, where it is possible to observe a slightly linear relation. Additionally, the ordinate at the origin is not zero, which indicates the existence of deviations from hydrodynamic behavior. Small deviations of this behavior have already been published in others studies with aluminum acetylacetonate in ethanol [104], gallic acid in ethanol [98], among others [60,102], under similar conditions.

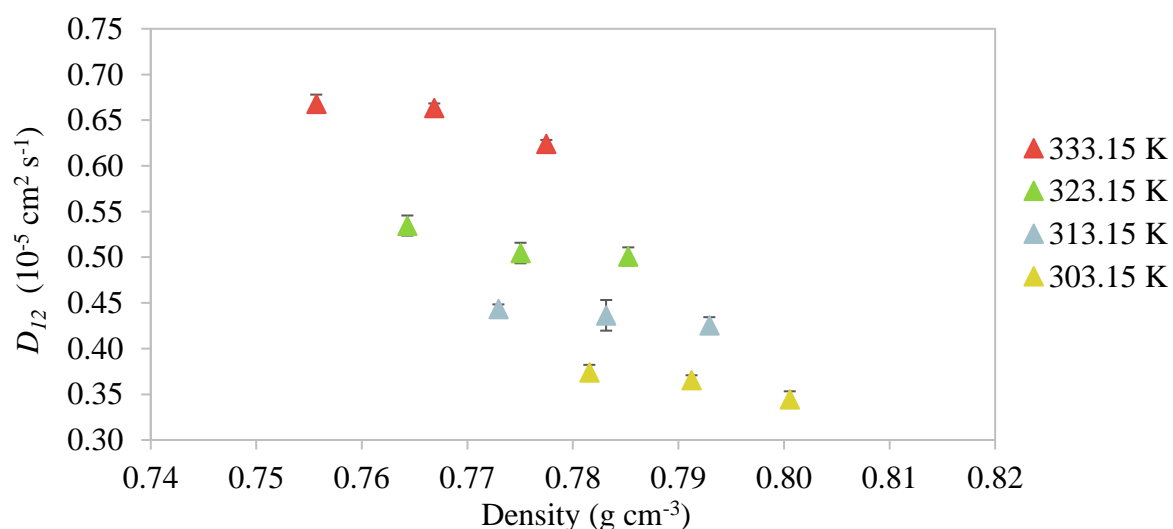


Figure 5.5- D_{12} of lycopene in ethanol as function of the solvent density for several temperatures.

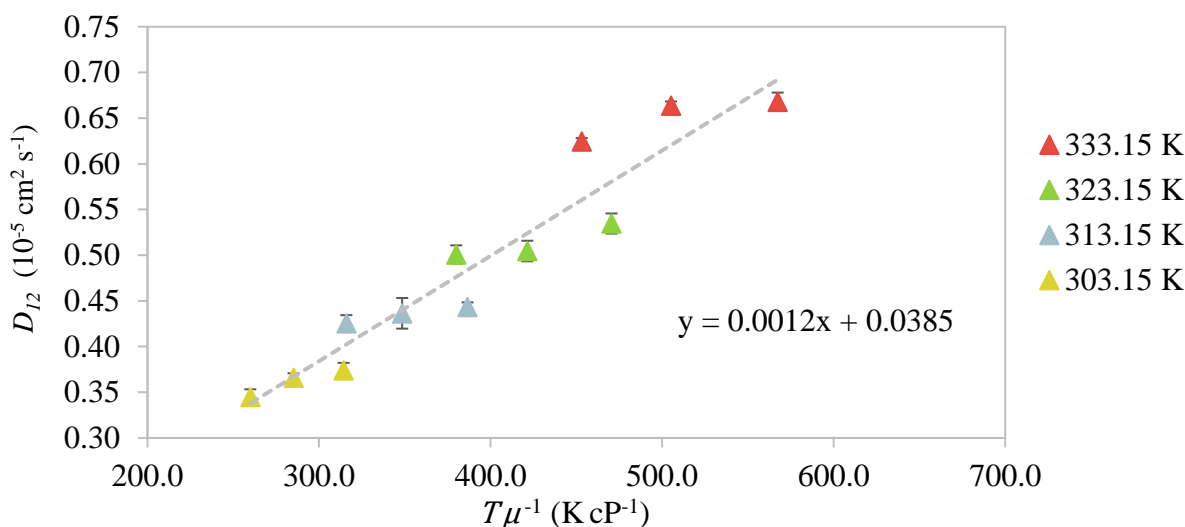


Figure 5.6- D_{12} of lycopene in ethanol plotted in Stokes-Einstein coordinates for several temperatures.

5.3 Tracer diffusivity of astaxanthin in ethyl acetate

As mentioned before, the reliable measurement of D_{12} is heavily linked with the analysis of the experimental absorbance profiles. Therefore, in order to select the optimal wavelength for the measurements, a wavelength study, similar to the one that was carried out for lycopene, was realized. Taking into account the absorbance spectrum of astaxanthin, which is presented in Appendix C, it is clear to see that the maximum absorbance is in the range of 420 to 500 nm. Accordingly, this was the range selected to conduct the study, which is compiled in Figure 5.7.

Analyzing Figure 5.7 it is possible to see that the whole wavelength range is quite stable and the minimum fitting error is achieved at 460 nm. Also, the D_{12} has a maximum variation of 3 %. Similarly to what has been done for lycopene (Chapter 5.2), more pulses were injected in this range of wavelengths to test the reproducibility of the results. Due to the good reproducibility and lowest fitting error obtained, the wavelength selected to perform the measurements was $\lambda = 460$ nm.

Beside the chosen concentration ($C = 0.20$ mg mL⁻¹), a smaller concentration ($C = 0.15$ mg mL⁻¹) was also tested. The values obtained using this lower concentration showed a small reproducibility and due to that, it was decided not to use it. No higher concentration was tested because the solubility of astaxanthin is very low [105] and its precipitation inside the diffusion column would block the equipment.

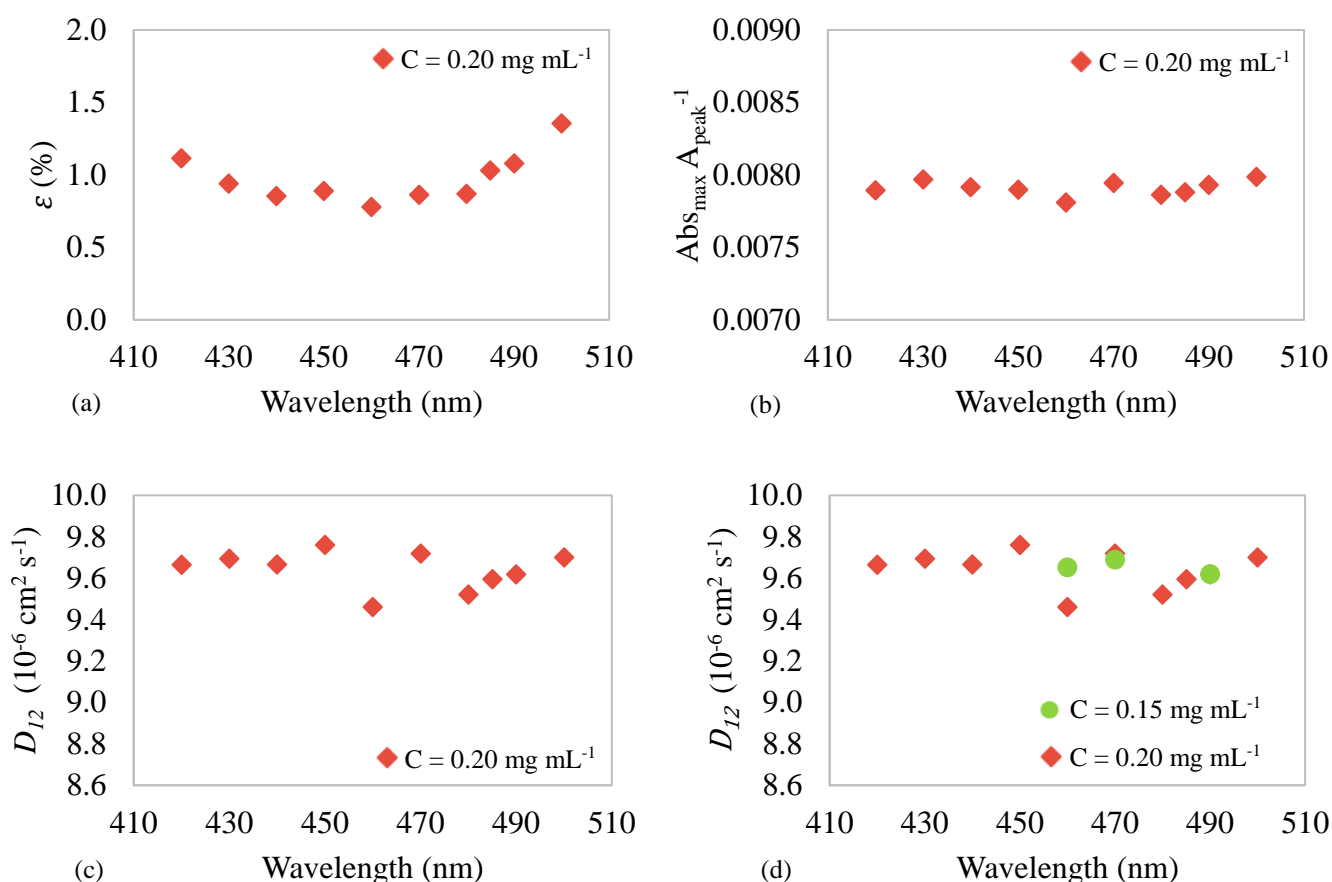


Figure 5.7- Determination of the optimal wavelength (λ) at 1 bar and 313.15 K, to study the diffusivity of astaxanthin in ethyl acetate. (a) Root mean square error *versus* λ , (b) Ratio of maximum absorbance to peak area ($\text{Abs}_{\text{max}} A_{\text{peak}}^{-1}$) *versus* λ , (c) Preliminary D_{12} *versus* λ and (d) Preliminary D_{12} *versus* λ for $C = 0.15 \text{ mg mL}^{-1}$ (●) and $C = 0.20 \text{ mg mL}^{-1}$ (◆).

The amount of solute injected in the column was $3.351 \times 10^{-4} \mu\text{mol}$, which ensures the infinite dilution conditions inside the column.

A typical response curve obtained for astaxanthin is shown in Figure 5.8, at 1 bar and 333.15 K. Similarly to the measurement of the D_{12} of lycopene, the applicability of the CPB method was assured in every assay, since the previously mentioned restrictions were fulfilled (Re ranged from 7.65 to 8.00; \bar{u} ranged from 1.14 to 1.20 cm s^{-1} ; Pe_x varied between 1.07×10^8 and 1.61×10^8 ; $D(\bar{u}L)^{-1} < 0.01$; $De\sqrt{Sc} < 10$; ε ranged from 0.52 to 2.10 % and the asymmetric factors of the peaks were close to one).

The obtained diffusivities of astaxanthin in ethyl acetate varied between 0.817×10^{-5} and $1.223 \times 10^{-5} \text{ cm}^2 \text{ s}^{-1}$, for a temperature range of 303.15 to 333.15 K and a pressure range of 1 to 100 bar. These values are reported in Table 5.3 and represented graphically in Figure 5.9 against pressure.

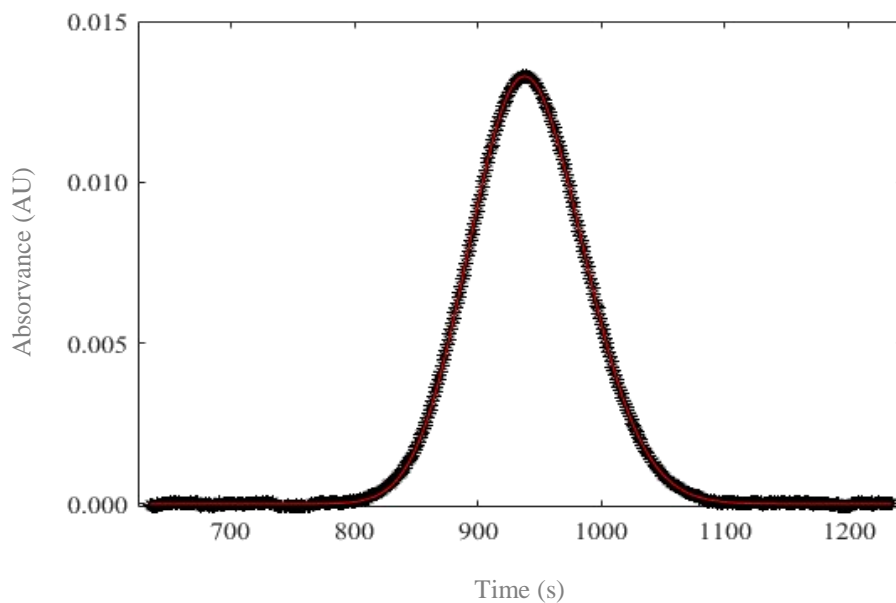


Figure 5.8- Experimental response curve (×) and calculated curve (–) for astaxanthin in ethyl acetate ($\lambda = 460$ nm) at 1 bar and 333.15 K

Table 5.3- Experimental conditions, experimental D_{12} of astaxanthin in ethyl acetate obtained through the CPB method and calculated density and viscosity of the solvent.

Temperature (K)	Pressure (bar)	$D_{12} \pm \Delta D_{12}$ ($10^{-5} \text{ cm}^2 \text{ s}^{-1}$)	Density (g cm^{-3})	Viscosity (cP)
303.15	1	0.842 ± 0.009	0.782	0.965
	50	0.831 ± 0.005	0.791	1.063
	100	0.817 ± 0.005	0.801	1.166
313.15	1	0.955 ± 0.011	0.773	0.810
	50	0.950 ± 0.001	0.783	0.899
	100	0.925 ± 0.002	0.793	0.991
323.15	1	1.102 ± 0.009	0.764	0.687
	50	1.075 ± 0.003	0.775	0.767
	100	1.034 ± 0.013	0.785	0.850
333.15	1	1.223 ± 0.012	0.756	0.587
	50	1.204 ± 0.011	0.767	0.659
	100	1.169 ± 0.004	0.777	0.735

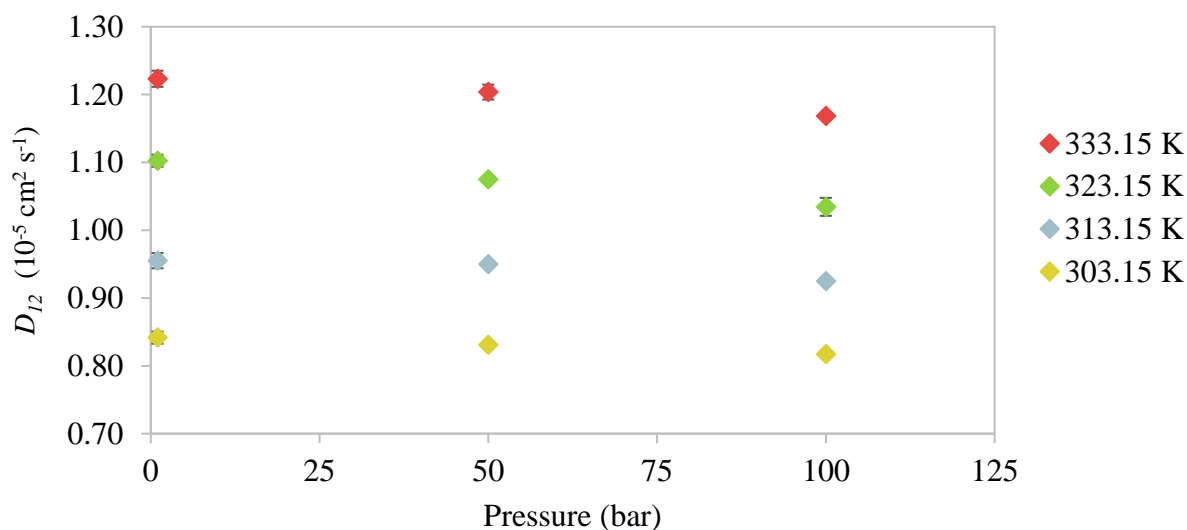


Figure 5.9- D_{12} of astaxanthin in ethyl acetate as function of pressure for several temperatures.

Taking a closer look to the data presented in Table 5.3 and Figure 5.9 is possible to see that the D_{12} of astaxanthin in ethyl acetate has a similar behavior of D_{12} of lycopene in ethanol. The decrease of D_{12} when pressure increases is in accordance with the free volume theories. At isobaric conditions, an increment of the temperature increases D_{12} . As explained in Chapter 5.2, this rise of D_{12} is due to the lower density (which increases the available free volume) and by the increase of the kinetic energy of the molecules of solute [64]. These recorded behaviors are consistent with results obtained for the D_{12} of lycopene as shown before, as well as the results reported in other works [43,78,98,103]. In Figure 5.10 is plotted the values of D_{12} versus density, where the negative effect that the increase of the density has on D_{12} is evident.

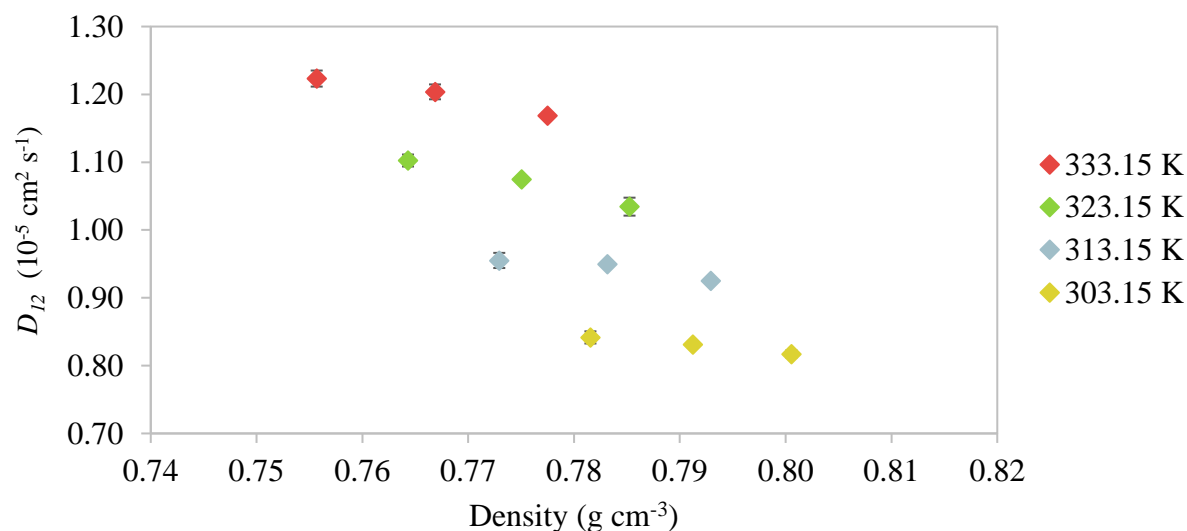


Figure 5.10- D_{12} of astaxanthin in ethyl acetate as function of the solvent density for several temperatures.

As well as for lycopene in ethanol, the hydrodynamic behavior of the system was also studied for astaxanthin. In Figure 5.11 are presented the data of D_{12} versus $T\mu^{-1}$, where it is possible to see a slightly linear relation. Furthermore, the non-zero ordinate at the origin indicates the existence of deviations from hydrodynamic behavior. As mentioned before, small deviations of this behavior have already been noticed in others studies [60,98,102,104].

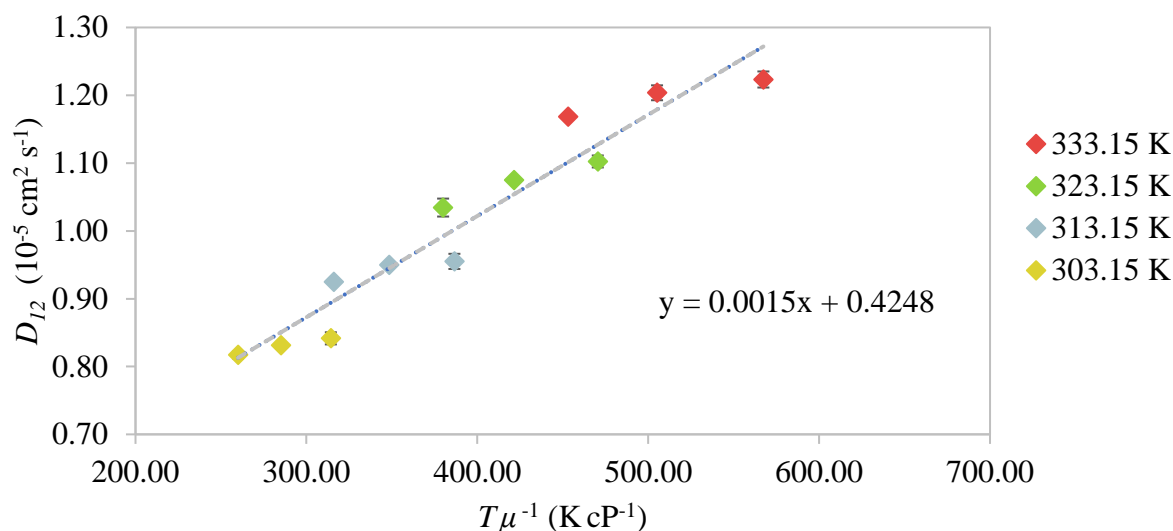


Figure 5.11- D_{12} of astaxanthin in ethyl acetate plotted in Stokes-Einstein coordinates for several temperatures.

5.4 Modeling the experimental values of D_{12}

To perform the modeling of the experimental D_{12} , one used the models presented in Chapter 3, with the exception of the Stokes-Einstein relation, which is only applicable to macroscopic systems, the Scheibel equation, since the restriction expressed in Eq. 3.10 was not fulfilled, and the Lai-Tan, because it was developed to supercritical fluids.

As mentioned before, the properties of the compounds of this thesis are presented in Appendix B.

In Table 5.4 are shown the modeling results and in Figure 5.12 they are compared with the experimental values of D_{12} .

Table 5.4- Modeling results of D_{12} of lycopene in ethanol and astaxanthin in ethyl acetate.

Model	No. parameters	Equation number	Lycopene in ethanol		Astaxanthin in ethyl acetate	
			Parameters	AARD (%)	Parameters	AARD (%)
DHB	2	3.2	$B_{DHB} = 4.800 \times 10^{-8} \text{ mol cm}^{-1} \text{ s}^{-1} \text{ K}^{-0.5}$ $V_D = 53.440 \text{ cm}^3 \text{ mol}^{-1}$	9.78	$B_{DHB} = 3.288 \times 10^{-8} \text{ mol cm}^{-1} \text{ s}^{-1} \text{ K}^{-0.5}$ $V_D = 82.830 \text{ cm}^3 \text{ mol}^{-1}$	4.81
Wilke-Chang	0	3.6 – 3.8	-	91.29	-	8.32
Tyn-Calus	0	3.11 – 3.14	-	63.67	-	72.96
Reddy-Doraiswamy	0	3.18 - 3.20	-	48.16	-	79.38
Catchpole-King	0	3.21 – 3.26	-	56.69	-	43.98
TLSM	0	3.27 – 3.37	-	9.68	-	27.51
TLSM _d	1	3.27 – 3.34	$k_{12,d} = -4.822 \times 10^{-2}$	6.92	$k_{12,d} = 1.440 \times 10^{-1}$	6.37
		3.38 – 3.39				
Empirical and semi-empirical correlations of Magalhães <i>et al.</i>	2	3.40	$a_3 = -0.883$ $b_3 = -6.661$	5.00	$a_3 = -0.600$ $b_3 = -6.323$	5.06
	2	3.41	$a_5 = 4.185 \times 10^{-6} \text{ cm}^2 \text{ cP s}^{-1}$ $b_5 = -2.244 \times 10^{-7} \text{ cm}^2 \text{ s}^{-1}$	6.35	$a_5 = 2.985 \times 10^{-6} \text{ cm}^2 \text{ cP s}^{-1}$ $b_5 = 2.422 \times 10^{-6} \text{ cm}^2 \text{ s}^{-1}$	7.29
	2	3.42	$a_7 = -1.882 \times 10^{-7} \text{ cm}^5 \text{ g}^{-1} \text{ K}^{-1} \text{ s}^{-1}$ $b_7 = 1.619 \times 10^{-7} \text{ cm}^2 \text{ K}^{-1} \text{ s}^{-1}$	8.92	$a_7 = -1.821 \times 10^{-7} \text{ cm}^5 \text{ g}^{-1} \text{ K}^{-1} \text{ s}^{-1}$ $b_7 = 1.921 \times 10^{-7} \text{ cm}^2 \text{ K}^{-1} \text{ s}^{-1}$	3.94
	2	3.43	$a_9 = -1.865 \times 10^{-8} \text{ cm}^5 \text{ g}^{-1} \text{ K}^{-1} \text{ s}^{-1}$ $b_9 = 2.768 \times 10^{-8} \text{ cm}^2 \text{ K}^{-1} \text{ s}^{-1} \text{ cP}$	6.60	$a_9 = -4.928 \times 10^{-8} \text{ cm}^5 \text{ g}^{-1} \text{ K}^{-1} \text{ s}^{-1}$ $b_9 = 4.889 \times 10^{-8} \text{ cm}^2 \text{ K}^{-1} \text{ s}^{-1} \text{ cP}$	5.03

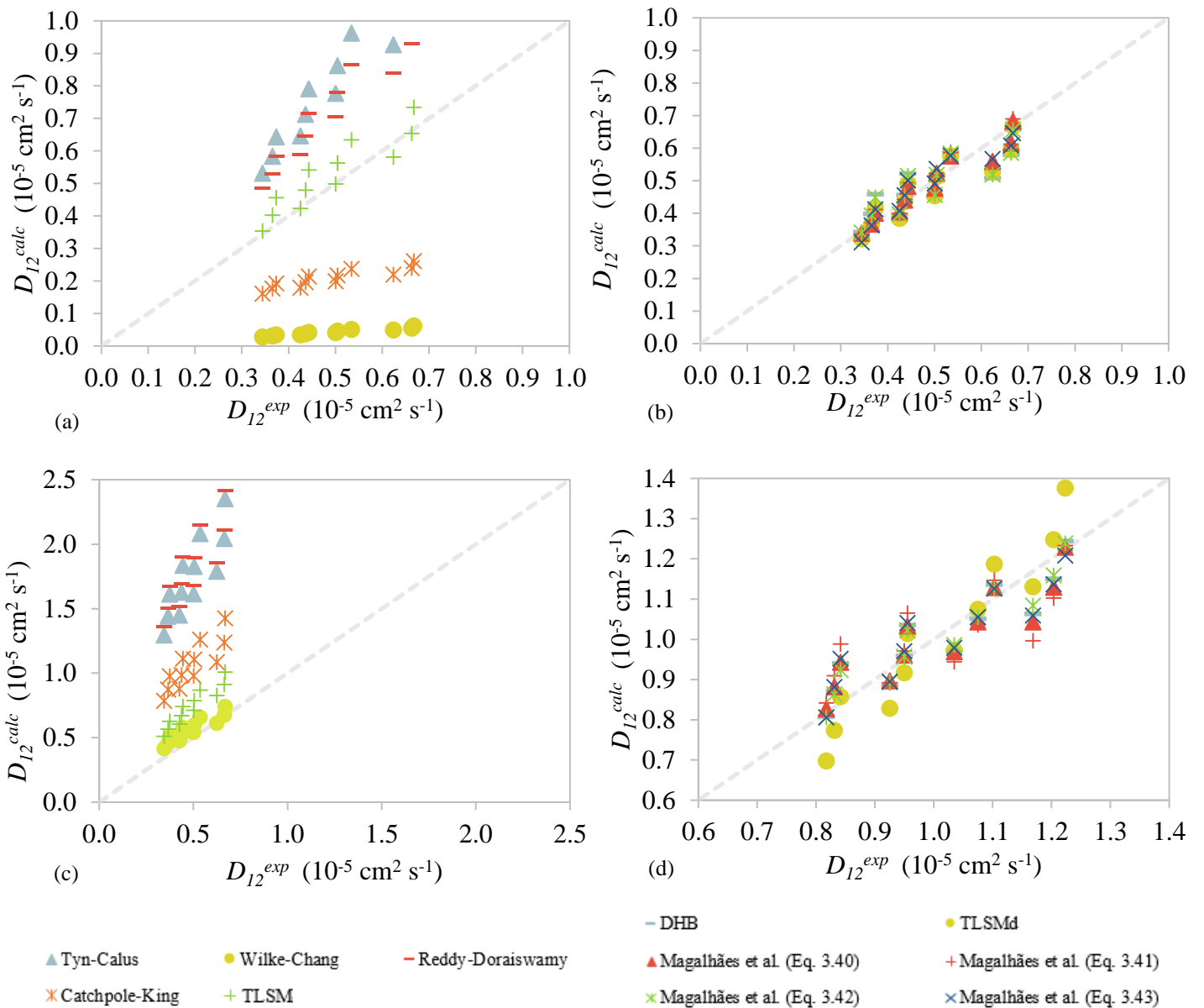


Figure 5.12- Calculated *versus* experimental values of D_{12} of lycopene in (a) and (b) and of astaxanthin in (c) and (d).

Analysing Figure 5.12 it is clear that very good results were achieved with the models of DHB, TLSM_d, and Magalhães *et al.* These models achieved AARDs of 9.78, 6.92 and 5.00 – 8.92 % for lycopene in ethanol, and 4.81, 6.37 and 3.94 – 7.29 % for astaxanthin in ethyl acetate, respectively.

The TLSM predictive model estimated the D_{12} of lycopene in ethanol reasonably well (AARD = 9.68 %), but not very well for astaxanthin in ethyl acetate (AARD = 27.51 %). This error is explained by the nature of the model, since it was developed for Lennard-Jones

fluids, *i.e.* when attractive forces are much weaker than the hydrogen bonds that astaxanthin can establish with ethyl acetate. It is also to notice that the introduction of one adjustable interaction parameter in the diameter combining rule, which produces the TL S M $_d$ model, allows the model to perform much better, since decreases the AARD from 27.51 to 6.37 % for astaxanthin.

The TL S M $_d$ model and the four correlations of Magalhães *et al.*, which require the knowledge of temperature and the density and viscosity of the solvent, achieved the best results, proving that these models are particularly appropriate to represent the diffusivity of either lycopene in ethanol or astaxanthin in ethyl acetate.

Chapter 6

Conclusion and future work suggestions

In this dissertation, the binary diffusion coefficient (D_{12}) of lycopene in ethanol and of astaxanthin in ethyl acetate were measured by the CPB method.

The influence of the wavelength on the diffusivity was firstly studied, in order to determine the best conditions to perform the measurements, and it was found that the optimal wavelengths were $\lambda = 255$ nm for lycopene and $\lambda = 460$ nm for astaxanthin.

The measurement of the diffusion coefficients of both systems took place in the range of 1-100 bar and of 303.15-333.15 K. The obtained diffusivities vary between 3.45×10^{-6} to 6.68×10^{-6} $\text{cm}^2 \text{s}^{-1}$ in the case of lycopene, and between 8.17×10^{-6} and 1.22×10^{-5} $\text{cm}^2 \text{s}^{-1}$ in the case of astaxanthin.

The experimental D_{12} was analyzed in terms of its dependency on pressure, temperature, density and Einstein-Stokes coordinates, and both systems exhibited the same behavior. This behavior was already expected and it is in accordance with the free volume theories.

In this work, the experimental results of D_{12} were also modeled using several predictive and correlation models, and relative deviations between 5.00 and 91.29 % were achieved for lycopene and between 3.94 and 79.38 % for astaxanthin. In general, very good results were obtained. The TL S M $_d$ model and the empirical and semi-empirical correlations Magalhães *et al.* proved to be the best equations, by presenting very small deviations (6.92 and 5.00 – 8.92 % for lycopene, respectively and 6.37 and 3.94 – 7.29 % for astaxanthin, respectively). Due to these low deviations, these models are particularly appropriate to represent the diffusivity of either lycopene or astaxanthin over the studied conditions.

Considering the overall benefits of the bioactive compounds and that they can be extracted and recovered from a wide range of sources, such as fruits, vegetables, algae, or even waste produced by the agroindustry and fishing industry, and the fact that the diffusion coefficient is an important property for process and equipment design and simulation, the

diffusivity of these compounds needs to be further studied, in particular the diffusivity of lycopene and astaxanthin in supercritical carbon dioxide (SC-CO₂) and in SC-CO₂ modified with cosolvents. Only a continuous study of the properties of bioactive compounds will allow the industry to replace the traditional extraction methods by more ecofriendly and modern techniques.

References

- [1] M. Ivanovi and M. E. Alañón, “Enhanced and green extraction of bioactive compounds from *Lippia citriodora* by tailor-made natural deep eutectic solvents,” *Food Res. Int.*, 111, 67–76, (2018).
- [2] C. M. G. C. Renard, “Extraction of bioactives from fruit and vegetables : State of the art and perspectives,” *LWT - Food Sci. Technol.*, 93, 390–395, (2018).
- [3] D. Pintac, T. Majkic, L. Torovic, D. Orcic, I. Beara, N. Mimica, and M. Lesjak, “Solvent selection for efficient extraction of bioactive compounds from grape pomace,” *Ind. Crop. Prod.*, 111, 379–390, (2018).
- [4] V. O. Monfi and S. Casas-Flores, “Molecular Mechanisms of Biocontrol in *Trichoderma* spp. and Their Applications in Agriculture,” in *Biotechnology and Biology of Trichoderma*, First Ed., United States of America: Elsevier, 2014, 429–454.
- [5] S. Vats, *Handbook of Food Bioengineering: Ingredients Extraction by Physicochemical Methods in Food*, Seventh ed. United States of America: Elsevier, 2017.
- [6] P. Kris-Etherton, K. D. Hecker, A. Bonanome, S. M. Coval, A. E. Binkoski, K. F. Hilpert, A. E. Griel, and T. D. Etherton, “Bioactive compounds in foods: Their role in the Prevention of Cardiovascular Disease and Cancer.,” *Am. J. Med.*, 113, 71S–88S, (2002).
- [7] M. Plaza, S. Santoyo, L. Jaime, G. García-Blairsy Reina, M. Herrero, F. J. Señoráns, and E. Ibáñez, “Screening for bioactive compounds from algae,” *J. Pharm. Biomed. Anal.*, 51, 450–455, (2010).
- [8] A. Ghasemzadeh and N. Ghasemzadeh, “Flavonoids and phenolic acids: Role and biochemical activity in plants and human,” *J. Med. Plants Res.*, 5, 6697–6703, (2011).
- [9] J. Giacometti, D. B. Kovacevic, P. Putnik, D. Gabric, T. Bilusic, and G. Kresic, “Extraction of bioactive compounds and essential oils from mediterranean herbs by

- conventional and green innovative techniques : A review,” *Food Res. Int.*, 113, 245–262, (2018).
- [10] N. S. Mashhadi, M. Zakerkish, J. Mohammadiasl, M. Zarei, M. Mohammadshahi, and M. H. Haghizadeh, “Astaxanthin improves glucose metabolism and reduces blood pressure in patients with type 2 diabetes mellitus,” *Asia Pac. J. Clin. Nutr.*, 27, 341–346, (2018).
- [11] M. I. Fernández-Mar, R. Mateos, M. C. García-Parrilla, B. Puertas, and E. Cantos-Villar, “Bioactive compounds in wine: Resveratrol, hydroxytyrosol and melatonin: A review,” *Food Chem.*, 130, 797–813, (2012).
- [12] F. Visioli, P. Riso, S. Grande, C. Galli, and M. Porrini, “Protective activity of tomato products on in vivo markers of lipid oxidation,” *Eur. J. Nutr.*, 42, 2003, 201–206.
- [13] M. H. Zainal-abidin, M. Hayyan, A. Hayyan, and N. S. Jayakumar, “New horizons in the extraction of bioactive compounds using deep eutectic solvents : A review,” *Anal. Chim. Acta*, 979, 1–23, (2017).
- [14] Grand View Research, “Bioactive Ingredients Market Analysis By Product (Fiber, Vitamin, Omega 3 PUFA, Plant Extract, Minerals, Carotenoids & Antioxidants, Probiotics), By Application (Functional Food & Beverages, Dietary Supplements, Clinical Nutrition, Personal Care) And Segm,” United States of America, (2016).
- [15] F. Chemat, M. A. Vian, and G. Cravotto, “Green extraction of natural products: concept and principles,” *Int. J. Mol. Sci.*, 13, 8615–8627, (2012).
- [16] M. Markom, H. Singh, and M. Hasan, “Supercritical CO₂ fractionation of crude palm oil,” *J. Supercrit. Fluids*, 20, 45–53, (2001).
- [17] M. N. Islam, Y. Jo, and J. Park, “Remediation of PAHs contaminated soil by extraction using subcritical water,” *J. Ind. Eng. Chem.*, 18, 1689–1693, (2012).
- [18] J. D. Seader, E. J. Henley, and D. K. Roper, *Separation Process Principles*, Third ed. United States of America: John Wiley & Sons, Inc., 2011.
- [19] F. P. Incropera, T. L. Bergman, A. S. Lavine, and D. P. DeWitt, *Fundamentals of Heat and Mass Transfer*, Seventh ed. United States of America: John Wiley & Sons, Inc., 2011.
- [20] E. L. Cussler, *Diffusion: Mass Transfer in Fluid Systems*, Third ed. New York: Cambridge University Press, 2009.
- [21] H. Klocker, H. Bart, R. Marr, and H. Muller, “Mass Transfer Based on Chemical

- Potential Theory: ZnSO₄/H₂SO₄/D₂EHPA,” *AIChE J.*, 43, 10, 2479–2487, (1997).
- [22] S. Voutilainen, T. Nurmi, J. Mursu, and T. H. Rissanen, “Carotenoids and cardiovascular health,” *Am. J. Clin. Nutr.*, 83, 1265–1271, (2006).
- [23] European Commission, “EU Approved additives and E Numbers,” Luxembourg, (2018).
- [24] U.S. Government, “Food and Drug Administration, HHS,” Washington DC, (2018).
- [25] H. D. Sesso, J. E. Buring, E. P. Norkus, and J. M. Gaziano, “Plasma lycopene , other carotenoids , and retinol and the risk of cardiovascular disease in men,” *Am. J. Clin. Nutr.*, 81, 990–997, (2005).
- [26] M. Kristenson, B. Ziedén, Z. Kucinskienė, L. S. Elinder, B. Bergdahl, B. Elwing, A. Abaravicius, L. Razinkovienė, H. Calkauskas, and A. G. Olsson, “Antioxidant state and mortality from coronary heart disease in Lithuanian and Swedish men: concomitant cross sectional study of men aged 50,” *Br. Med. J.*, 314, 629–633, (1997).
- [27] K. S. C. Bose and B. K. Agrawal, “Effect of lycopene from cooked tomatoes on serum antioxidant enzymes, lipid peroxidation rate and lipid profile in coronary heart disease,” *Singapore Med. J.*, 48, 415–420, (2007).
- [28] A. Agarwal, M. A. H. Shen, S. Agarwal, and A. V. Rao, “Lycopene Content of Tomato Products: Its Stability, Bioavailability and In Vivo Antioxidant Properties,” *J. Med. Food*, 4, 9–15, (2001).
- [29] A. Dasgupta and K. Klein, *Antioxidants in Food, Vitamins and Supplements: Prevention and Treatment of Disease*, First Ed. United States of America: Elsevier, 2014.
- [30] European Commission, “Monitoring EU Agri-Food Trade: Tomatoes Dashboard Reports,” Luxembourg, (2018).
- [31] Y. M. A. Naguib, “Antioxidant activities of astaxanthin and related carotenoids,” *J. Agric. Food Chem.*, 48, 2000, 1150–1154.
- [32] T. Iwamoto, K. Hosoda, R. Hirano, H. Kurata, A. Matsumoto, W. Miki, M. Kamiyama, H. Itakura, S. Yamamoto, and K. Kondo, “Inhibition of Low-Density Lipoprotein Oxidation by Astaxanthin,” *J. Atherosclerosis Thromb.*, 7, 216–222, (2000).
- [33] G. Riccioni, “Carotenoids and Cardiovascular Disease,” *Curr. Atheroscler. Rep.*, 11, 434–439, (2009).

- [34] European Commission, “Factos e números sobre a política comum das pescas,” Belgium, (2016).
- [35] K. K. Liong, P. A. Wells, and N. R. Foster, “Diffusion in supercritical fluids,” *J. Supercrit. Fluids*, 4, 91–108, (1991).
- [36] T. Funazukuri, C. Yi, and S. Kagei, “Impulse response techniques to measure binary diffusion coefficients under supercritical conditions,” *J. Chromatogr. A*, 1037, 411–429, (2004).
- [37] O. J. Catchpole and M. B. King, “Measurement and correlation of binary diffusion coefficients in near critical fluids,” *Ind. Eng. Chem. Res.*, 33, 7, 1828–1837, (1994).
- [38] C.-C. Lai and C.-S. Tan, “Measurement of molecular diffusion coefficient in supercritical carbon dioxide using a coated capillary column,” *Ind. Eng. Chem. Res.*, 34, 3, 674–680, (1995).
- [39] G. Taylor, “Diffusion and mass transport in tubes,” *Proc. Phys. Soc.*, LXVII, 12–B, 857–869, (1954).
- [40] G. Taylor, “Conditions under which dispersion of a solute in a stream of solvent can be used to measure molecular diffusion,” *Proc. R. Soc. A Math. Phys. Eng. Sci.*, 225, 1163, 473–477, (1954).
- [41] G. Taylor, “Dispersion of soluble matter in solvent flowing slowly through a tube,” *Proc. R. Soc. A Math. Phys. Eng. Sci.*, 219, 1137, 186–203, (1953).
- [42] R. Aris, “On the dispersion of a solute in a fluid flowing through a tube,” *Process Syst. Eng.*, 1, C, 109–120, (1999).
- [43] C. M. Silva and E. A. Macedo, “Diffusion coefficients of ethers in supercritical carbon dioxide,” *Ind. Eng. Chem. Res.*, 37, 4, 1490–1498, (1998).
- [44] J. C. Giddings and S. L. Seager, “Method for rapid determination of diffusion coefficients,” *Ind. Eng. Chem. Fundam.*, 1, 4, 277–283, (1962).
- [45] Z. Balenovic, M. N. Myers, and J. Calvin Giddings, “Binary diffusion in dense gases to 1360 atm by the chromatographic peak-broadening method,” *J. Chem. Phys.*, 52, 2, 915–922, (1970).
- [46] A. C. Ouano, “Diffusion in liquid systems. I. A simple and fast method of measuring diffusion constants,” *Ind. Eng. Chem. Fundam.*, 11, 2, 268–271, (1972).
- [47] I. Swaid and G. M. Schneider, “Determination of binary diffusion coefficients of benzene and some alkylbenzenes in supercritical CO₂ between 308 and 328 K in the

- pressure range 80 to 160 bar with supercritical fluid chromatography (SFC),” *Berichte der Bunsengesellschaft/Physical Chem. Chem. Phys.*, **83**, 10, 969–974, (1979).
- [48] J. M. H. Levelt Sengers, U. K. Deiters, U. Klask, P. Swidersky, and G. M. Schneider, “Application of the Taylor dispersion method in supercritical fluids,” *Int. J. Thermophys.*, **14**, 4, 893–922, (1993).
- [49] C. M. Silva, “Coeficientes de difusão em misturas supercríticas,” Faculdade de Engenharia da Universidade do Porto, 1998.
- [50] J. A. Moulijn, R. Spijker, and J. F. M. Kolk, “Axial dispersion of gases flowing through coiled columns,” *J. Chromatogr. A*, **142**, C, 155–166, (1977).
- [51] R. Aris, *Mathematical Modeling: A Chemical Engineer’s Perspective*. San Diego, California: Academic Press, 1999.
- [52] O. Levenspiel, *Chemical Reaction Engineering*, Third ed. New York: John Wiley & Sons, Inc., 1999.
- [53] L. Sharma, K. D. P. Nigam, and S. Roy, “Single phase mixing in coiled tubes and coiled flow inverters in different flow regimes,” *Chem. Eng. Sci.*, **160**, April 2016, 227–235, (2017).
- [54] R. J. Nunge, T. S. Lin, and W. N. Gill, “Laminar dispersion in curved tubes and channels,” *J. Fluid Mech.*, **51**, 2, 363–383, (1972).
- [55] A. Alizadeh, C. A. Nieto de Castro, and W. A. Wakeham, “The theory of the Taylor dispersion technique for liquid diffusivity measurements,” *Int. J. Thermophys.*, **1**, 3, 243–284, (1980).
- [56] T. Funazukuri, C. Y. Kong, and S. Kagei, “Infinite-dilution binary diffusion coefficients of 2-propanone, 2-butanone, 2-pentanone, and 3-pentanone in CO₂ by the Taylor dispersion technique from 308.15 to 328.15 K in the pressure range from 8 to 35 MPa,” *Int. J. Thermophys.*, **21**, 6, 2–3, (2000).
- [57] E. T. van der Laan, “Notes on the diffusion type model for longitudinal mixing in flow,” *Chem. Eng. Sci.*, **7**, 187, (1958).
- [58] W. A. Wakeham, A. Nagashima, and J. V. Sengers, *Measurement of the Transport Properties of Fluids*. Cornwall: Blackwell Scientific Publications, 1991.
- [59] C. Yi, T. Funazukuri, and S. Kagei, “Chromatographic impulse response technique with curve fitting to measure binary diffusion coefficients and retention factors using polymer-coated capillary columns,” *J. Chromatogr. A*, **1035**, 177–193, (2004).

- [60] R. V Vaz, A. L. Magalhães, A. A. Valente, and C. M. Silva, “Measurement and modeling of tracer diffusivities of α -pinene in supercritical CO₂, and analysis of their hydrodynamic and free-volume behaviors,” *J. Supercrit. Fluids*, 107, 690–698, (2016).
- [61] J. Cordeiro, A. L. Magalhães, A. A. Valente, and C. M. Silva, “Experimental and theoretical analysis of the diffusion behavior of chromium(III) acetylacetonate in supercritical CO₂,” *J. Supercrit. Fluids*, 118, 153–162, (2016).
- [62] C. M. Silva, C. A. Filho, M. B. Quadri, and E. A. Macedo, “Binary diffusion coefficients of α -pinene and β -pinene in supercritical carbon dioxide,” 32, 167–175, (2004).
- [63] R. Lin and L. L. Tavlarides, “Diffusion coefficients of diesel fuel and surrogate compounds in supercritical carbon dioxide,” *J. Supercrit. Fluids*, 52, 47–55, (2010).
- [64] I. Medina, “Determination of diffusion coefficients for supercritical fluids,” *J. Chromatogr. A*, 1250, 124–140, (2012).
- [65] T. Funazukuri, C. Yi, and S. Kagei, “Measurements of binary diffusion coefficients for some low volatile compounds in supercritical carbon dioxide by input–output response technique with two diffusion columns connected in series,” *Fluid Phase Equilib.*, 197, 1169–1178, (2002).
- [66] L. M. Gonza, J. L. Bueno, and I. Medina, “Measurement of diffusion coefficients for 2-nitroanisole, 1,2-dichlorobenzene and *tert*-butylbenzene in carbon dioxide containing modifiers,” *J. Supercrit. Fluids*, 24, 219–229, (2002).
- [67] G. Madras, B. L. Hamilton, and M. A. Matthews, “Influence of adsorption on the measurement of diffusion coefficients by Taylor dispersion,” *Int. J. Thermophys.*, 17, 2, 17, (1996).
- [68] C. Yi, T. Funazukuri, S. Kagei, G. Wang, and F. Lu, “Applications of the chromatographic impulse response method in supercritical fluid chromatography,” *J. Chromatogr. A*, 1250, 141–156, (2012).
- [69] C. R. Wilke and P. Chang, “Correlation of diffusion coefficients in dilute solutions,” *A.I.Ch.E. J.*, 1, 2, 264–270, (1955).
- [70] B. E. Poling, J. M. Prausnitz, and J. P. O’Connell, *The Properties of Gases and Liquids*, Fifth ed. The McGraw-Hill Companies, Inc, 2001.
- [71] P. F. Lito, A. L. Magalhães, J. R. B. Gomes, and C. M. Silva, “Universal model for

- accurate calculation of tracer diffusion coefficients in gas, liquid and supercritical systems,” *J. Chromatogr. A*, 1290, 1–26, (2013).
- [72] C. M. Silva and H. Liu, “Modelling of Transport Properties of Hard Shpere Fluids and Related Systems, and its Applications,” in *Theory and Simulation of Hard Sphere Fluids and Related Systems*, 753, Berlin: Springer, 2008, 383–492.
- [73] J. R. Heirtzler and R. H. Burroughs, “Motions of molecules in liquids : Viscosity and diffusivity,” *Science*, 174, 0–3, (1971).
- [74] J. H. Dymond, “Corrected Enskog theory and the transport coefficients of liquids,” *J. Chem. Phys.*, 60, 969, (1974).
- [75] S. Chen, H. T. Davis, and D. F. Evans, “Tracer diffusion in polyatomic liquids. III,” *J. Chem. Phys.*, 77, 2540, (1982).
- [76] H. Liu, C. M. Silva, and E. A. Macedo, “New equations for tracer diffusion coefficients of solutes in supercritical and liquid solvents based on the Lennard-Jones fluid model,” *Ind. Eng. Chem. Res.*, 36, 1, 246–252, (1997).
- [77] J. Millat, J. H. Dymond, and C. A. Nieto de Castro, *Transport Properties of Fluids: Their Correlation, Prediction and Estimation*. New York: Cambridge University Press, 1996.
- [78] B. Zêzere, A. L. Magalhães, and C. M. Silva, “Diffusion coefficients of eucalyptol at infinite dilution in compressed liquid ethanol and in supercritical CO₂/ethanol mixtures,” *J. Supercrit. Fluids*, 133, 297–308, (2018).
- [79] H. Mehrer, *Diffusion in Solids Fundamentals, Methods, Materials, Diffusion-Controlled Processes*. Springer, 2007.
- [80] A. S. Parmar and M. Muschol, “Lysozyme as diffusion tracer for measuring aqueous solution viscosity,” *J. Colloid Interface Sci.*, 339, 1, 243–248, (2009).
- [81] J. J. Brey and J. G. Ordóñez, “Computer studies of Brownian motion in a Lennard-Jones fluid: The Stokes law,” *J. Chem. Phys.*, 76, 6, 3260–3263, (1982).
- [82] R. H. Perry, D. W. Green, and J. O. Maloney, *Perry’s Chemical Engineers’ Handbook*, Seventh ed. The McGraw-Hill Companies, Inc, 1997.
- [83] E. G. Scheibel, “Liquid Diffusivities,” *Ind. Eng. Chem.*, 2007–2008, (1954).
- [84] R. V. Vaz, A. L. Magalhães, and C. M. Silva, “Improved hydrodynamic equations for the accurate prediction of diffusivities in supercritical carbon dioxide,” *Fluid Phase Equilib.*, 360, 401–415, (2013).

- [85] K. A. Reddy and L. K. Doraiswamy, “Estimating liquid diffusivity,” *Ind. Eng. Chem. Fundam.*, 6, 1, 77–79, (1967).
- [86] H. Van Beijeren and M. H. Ernst, “The modified Enskog equation,” *Physica*, 68, 437–456, (1973).
- [87] L. Barajas, L. S. García-Colín, and E. Piña, “On the Enskog-Thorne theory for a binary mixture of dissimilar rigid spheres,” *J. Statistical Phys.*, 7, 2, 161–183, (1973).
- [88] E. N. Fuller, P. D. Schettler, and J. C. Giddings, “A new method for prediction of binary gas-phase diffusion coefficients,” *Ind. Eng. Chem. Fundam.*, 58, 5, 19–27, (1966).
- [89] A. L. Magalhães, S. P. Cardoso, B. R. Figueiredo, F. A. Da Silva, and C. M. Silva, “Revisiting the Liu-Silva-Macedo model for tracer diffusion coefficients of supercritical, liquid, and gaseous systems,” *Ind. Eng. Chem. Res.*, 49, 16, 7697–7700, (2010).
- [90] A. L. Magalhães, P. F. Lito, F. A. Da Silva, and C. M. Silva, “Simple and accurate correlations for diffusion coefficients of solutes in liquids and supercritical fluids over wide ranges of temperature and density,” *J. Supercrit. Fluids*, 76, 94–114, (2013).
- [91] C. Yin, S. Yang, X. Liu, and H. Yan, “Efficient extraction of astaxanthin from *phaffia rhodozyma* with polar and non-polar solvents after acid washing,” *Chinese J. Chem. Eng.*, 21, 2013, 776–780.
- [92] M. M. Calvo, D. Dado, and G. Santa-María, “Influence of extraction with ethanol or ethyl acetate on the yield of lycopene, β -carotene, phytoene and phytofluene from tomato peel powder,” *Eur. Food Res. Technol.*, 224, 2007, 567–571.
- [93] J. H. Dymond and R. Malhotra, “The Tait equation: 100 Years On,” *Int. J. Thermophys.*, 9, 6, 941–951, (1988).
- [94] A. Kumagai and H. Iwasaki, “Pressure-volume-temperature relationships of $\text{CH}_3\text{COOC}_2\text{H}_5$, and generalized Tait equation for liquids at high pressures,” *J. Chem. Eng. Data*, 24, 261–263, (1979).
- [95] J. J. Cano-Gómez, G. A. Iglesias-Silva, V. Rico-Ramírez, M. Ramos-Estrada, and K. R. Hall, “A new correlation for the prediction of refractive index and liquid densities of 1-alcohols,” *Fluid Phase Equilib.*, 387, 117–120, (2015).
- [96] J. J. Cano-Gómez, G. A. Iglesias-Silva, and M. Ramos-Estrada, “Correlations for the prediction of the density and viscosity of 1-alcohols at high pressures,” *Fluid Phase*

- Equilib.*, 404, 109–117, (2015).
- [97] C. L. Yaws, *Chemical Properties Handbook*, First ed. New York: McGraw-Hill Education, 1998.
- [98] J. Leite, A. L. Magalhães, A. A. Valente, and C. M. Silva, “Measurement and modelling of tracer diffusivities of gallic acid in liquid ethanol and in supercritical CO₂ modified with ethanol,” *J. Supercrit. Fluids*, 131, 130–139, (2018).
- [99] N. E. Craft and J. H. Soares, “Relative solubility, stability, and absorptivity of lutein and β -carotene in organic solvents,” *J. Agric. Food Chem.*, 40, 431–434, (1992).
- [100] E. Luengo, I. Álvarez, and J. Raso, “Improving carotenoid extraction from tomato waste by pulsed electric fields,” *Front. Nutr.*, 1, 1–10, (2014).
- [101] H. Liu, C. M. Silva, and E. A. Macedo, “Unified approach to the self-diffusion coefficients of dense fluids over wide ranges of temperature and pressure - hard-sphere, square-well, Lennard-Jones and real substances,” *Chem. Eng. Sci.*, 53, 2403–2422, (1998).
- [102] C. M. Silva, H. Liu, and E. A. Macedo, “Models for self-diffusion coefficients of dense fluids, including hydrogen-bonding substances,” *Chem. Eng. Sci.*, 53, 2423–2429, (1998).
- [103] T. Funazukuri, T. Sugihara, K. Yui, T. Ishii, and M. Taguchi, “Measurement of infinite dilution diffusion coefficients of Vitamin K3 in CO₂ expanded methanol,” *J. Supercrit. Fluids*, 108, 19–25, (2016).
- [104] C. Y. Kong, K. Watanabe, and T. Funazukuri, “Determination and correlation of infinite dilution binary diffusion coefficients for aluminum acetylacetonate in supercritical and liquid fluids,” *Fluid Phase Equilib.*, 420, 83–88, (2015).
- [105] J. Jorge, “Micronization of astaxanthin by the supercritical anti-solvent process (SAS),” 2014.

Appendix A

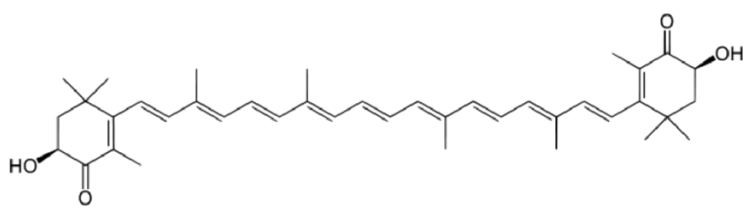
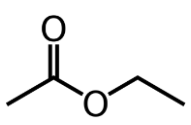
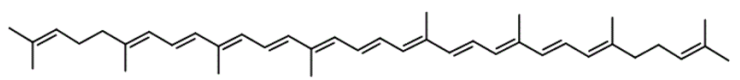
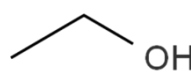
Chemical compounds

In this section are presented the chemical compounds used in this work, as well as a brief summary of their information.

Table A. 1- List of the chemical compounds used in the experimental work.

Compound	Molecular formula	CAS number	Molecular weight (g mol ⁻¹)	Supplier	Purity (%)
Astaxanthin	C ₄₀ H ₅₂ O ₄	472-61-7	596.84	Sigma-Aldrich	97.00
Ethanol	C ₂ H ₅ OH	64-17-5	46.069	Fisher Chemical	99.99
Ethyl acetate	C ₄ H ₈ O ₂	141-78-6	88.105	CARLO ERBA Reagents S.A.S	99.99
Lycopene	C ₄₀ H ₅₆	502-65-8	536.89	AKSci	85.00

Table A. 2- Structural formulas of the compounds used in the experimental work.

Astaxanthin	Ethyl acetate
	
Lycopene	Ethanol
	

Appendix B

Properties estimation

In this section are presented the properties of the compounds used in this work, which were used during the modeling of the obtained results.

Table B. 1- Properties of the chemical compounds used in this work.

Compound	M_i (g mol ⁻¹)	p_c (bar)	T_b (K)	T_c (K)	V_c (cm ³ mol ⁻¹)	V_d (cm ³)	V_i (cm ³ mol ⁻¹)	σ_{LJ} (Å)	$\frac{\varepsilon_{LJ}}{k_B}$ (K)
Astaxanthin	596.84 ^a	5.30 ^c	1047.00 ^c	1148.51 ^c	1877.50 ^c	539.30 ^d	768.34 ^e	9.9803 ^f	1004.60 ^f
Ethanol	46.07 ^b	63.84 ^b	351.44 ^b	516.25 ^b	166.90 ^b	51.77 ^d	60.81 ^e	4.5180 ^f	399.58 ^f
Ethyl acetate	88.11 ^b	38.80 ^b	350.21 ^b	523.30 ^b	286.00 ^b	94.30 ^d	106.93 ^e	5.3148 ^f	405.03 ^f
Lycopene	536.87 ^a	7.02 ^c	934.00 ^c	1297.93 ^c	2023.50 ^c	765.36 ^d	831.08 ^e	10.2325 ^f	888.96 ^f

^a Taken from the safety data sheet from the supplier, ^b Taken from the “Chemical Properties Handbook” [97], ^c Estimated through the Joback’s method [97], ^d Taken from “The Properties of Gases and Liquids” [70], ^e Estimated through Eq. 3.7 and ^f Taken from “Modelling of Transport Properties of Hard Shpere Fluids and Related Systems, and its Applications” [72].

Appendix C

Absorbance spectra

In this section are presented the absorbance spectra of lycopene and astaxanthin.

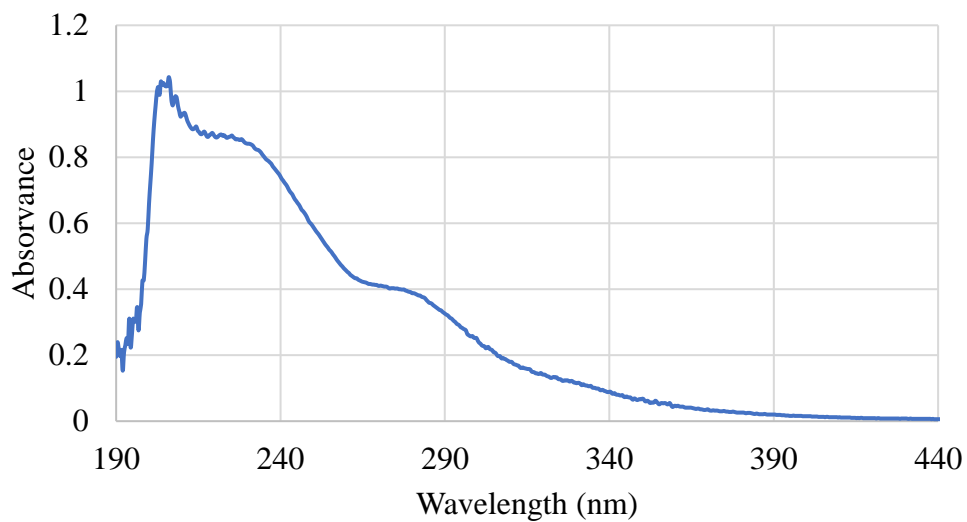


Figure C. 1- Lycopene absorbance spectrum ranging from 190 to 440 nm.

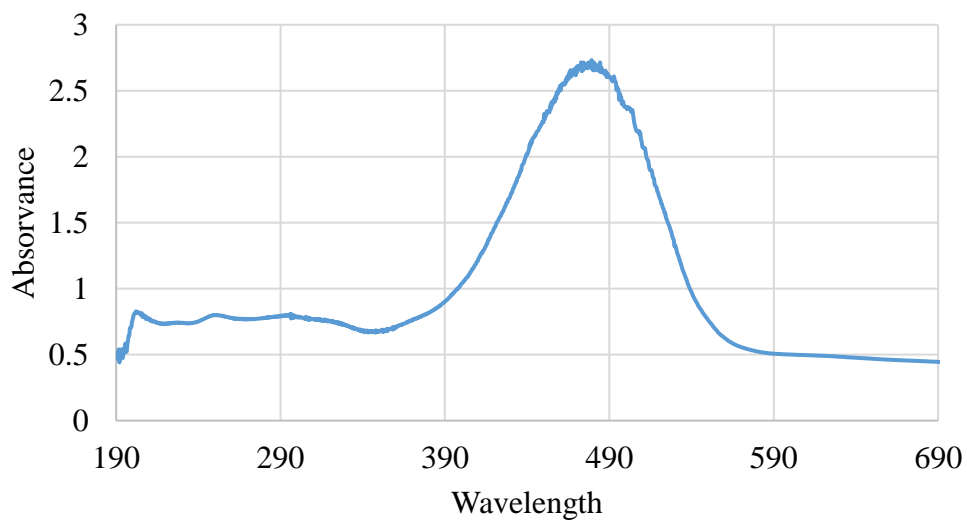


Figure C. 2- Astaxanthin absorbance spectrum ranging from 190 to 690 nm.